FISEVIER

Contents lists available at ScienceDirect

# Journal of Sound and Vibration

journal homepage: www.elsevier.com/locate/jsvi



# Iterative nonlinear chirp mode decomposition: A Hilbert-Huang transform-like method in capturing intra-wave modulations of nonlinear responses



Guowei Tu <sup>a</sup>, Xingjian Dong <sup>a, \*</sup>, Shiqian Chen <sup>b</sup>, Baoxuan Zhao <sup>a</sup>, Lan Hu <sup>c</sup>, Zhike Peng <sup>a</sup>

- <sup>a</sup> State Key Laboratory of Mechanical System and Vibration, Shanghai Jiao Tong University, Shanghai, 200240, China
- <sup>b</sup> State Key Laboratory of Traction Power, Southwest Jiaotong University, Chengdu, 610031, China
- <sup>c</sup> Shanghai Aerospace Equipments Manufacturer Co. Ltd., Shanghai, 200245, China

#### ARTICLE INFO

# Article history: Received 20 February 2020 Received in revised form 23 May 2020 Accepted 4 July 2020 Available online 12 July 2020 Handling Editor: K. Shin

Keywords:
Intra-wave modulation
Hilbert-Huang transform
Nonlinear chirp mode decomposition
Nonlinear system identification

#### ABSTRACT

Intra-wave modulations are a class of inherent nonlinear characteristics, exhibiting a fast oscillating instantaneous frequency and/or amplitude of responses. With the aid of the well-known Hilbert-Huang transform (HHT), such phenomena have been observed and utilized in many practical nonlinear systems including mechanical, power, ocean and even human biological systems. However, the empirical nature of the HHT makes the results physically uninterpretable and sensitive to perturbations of noise. Variational nonlinear chirp mode decomposition (VNCMD) is a recently proposed tool for analyzing wideband multicomponent signals, including intra-wave modulated responses. On the other hand, the VNCMD has strict requirements on the priori information of the signal. In this paper, we combine the framework of the VNCMD with that of the HHT, by replacing the jointoptimization scheme of the VNCMD with a recursive procedure adopted in the HHT. In this way, the new method becomes more adaptive without losing the rigorous mathematical foundation. This construction leads to a descendant of VNCMD, named the iterative nonlinear chirp mode decomposition (INCMD). Through dynamic simulations and applications to real data, it is demonstrated that the INCMD considerably outperforms state-of-the-art techniques of the same class. Using the INCMD, intra-wave modulations can be captured with high accuracy and strong noise-robustness, Extracted modulation features by the INCMD greatly help to detect and identify nonlinear systems.

© 2020 Elsevier Ltd. All rights reserved.

#### 1. Introduction

Understanding the intrinsic physical processes underlying nonlinear phenomena has always been a key issue in nonlinear dynamics. Solutions of the corresponding inverse problems are generally required to gain new insights into a certain nonlinear effect. In this sense, signal processing plays an important role since it can be utilized in system identification, a well-known inverse problem. Dualities between forward and inverse problems exist [1]: The classic Poincaré's perturbation

<sup>\*</sup> Corresponding author.

E-mail address: donxij@sjtu.edu.cn (X. Dong).

#### Nomenclature

ADMM Alternating direction method of multipliers

AM Amplitude modulation
DOF Single-degree-of-freedom
EMD Empirical mode decomposition
EWT Empirical wavelet transform
FM Frequency modulation

F-SST Short-time Fourier transform-based synchrosqueezing transform

HB Harmonic balance HHT Hilbert-Huang transform IA Instantaneous amplitude

ICCD Intrinsic chirp component decomposition

IF Instantaneous frequency IMF Intrinsic mode function

INCMD Iterative nonlinear chirp mode decomposition

**KBM** Krylov-Bogoliubov-Mitropolsky M-DOF Multi-degree-of-freedom **NCM** Nonlinear chirp mode **PSD** Power spectral density **RMSE** Root mean square error S-DOF Single-degree-of-freedom **SNR** Signal-to-noise ratio SST Synchrosqueezing transform **STFT** Short-time Fourier transform **TFA** Time-frequency analysis **TFD** Time-frequency distribution

VMD Variational mode decomposition
VNCMD Variational nonlinear chirp mode decomposition
W-SST Wavelet transform-based synchrosqueezing transform

WT Wavelet transform

method adopts a formal power series to quantify the small deviation from the solvable linear to the unsolvable nonlinear system, and this deviation relates to the harmonic distortion in temporal waves, one of the clearest nonlinearity indicators [2]; Fourier analysis further can reveal super- and/or sub-harmonics, another well-known nonlinearity indicator already utilized in many practical engineering issues [3], and the basic idea of this tool coincides with that of the harmonic balance (HB), a frequency-domain based-method to calculate the steady-state of nonlinear systems [4]. Two types of dualities above capture the basic characteristics of nonlinear responses [1].

Combining the time and the frequency domain description, the time-frequency analysis (TFA) techniques are used to observe the response in a joint domain [5]. In this vein, some time-varying features such as skeleton curves [6], instantaneous modal parameters [7] and resonance transitions [8] can be tracked using some common TFA methods like the short-time Fourier transform (STFT) and the wavelet transform (WT) [9]. What's worth noting is that nonlinear features mentioned above are slow dynamics deriving a system with slowly-varying amplitudes and phases [10], which can also be obtained by the method of averaging, the Krylov-Bogoliubov-Mitropolsky (KBM) approach or the multiple-scale analysis [4] analytically. Opposed to this, a class of fast dynamics termed the intra-wave modulations, exhibiting a fast oscillating instantaneous frequency (IF) and/or amplitude (IA) in the time-frequency-energy domain, were first observed by Huang et al. (1996) [11] when he employed the Hilbert-Huang transform (HHT) method to analyze classic nonlinear systems including the Duffing, Lorenz, and Rössler systems. As Huang pointed out [11], instead of interpreting the dispersive propagation externally shown in a wave train, which should be regarded as the inter-wave modulation, the intra-wave modulation captures an inherent nonlinearity connected to harmonic distortions. Intra-wave modulations ought to make physical sense and provide more detailed information than modern topological tools can do. Such characteristics, however, are lost in Fourier analysis and vaguely depicted by wavelet analysis [11].

No rigorous analysis directly derives such fast dynamics though, it has been demonstrated that the intra-wave modulation originates from classic perturbations under specific approximations [12], and Bessel functions describe the quantitative relationship between modulation features and the harmonic distortion [1]. Following Huang's study, researchers have noticed similar phenomena in many practical nonlinear systems such as rotor systems with rubbing [13] or crack fault [14], non-stationary power systems [15], ocean systems [16], and even human biological systems [17,18]: the intra-wave

modulation comes into being along with the emergence of nonlinearity, making itself a novel tool for nonlinearity detections and identifications [13].

However, the empirical nature of the HHT method prohibits new insights into this nonlinear phenomenon. The HHT adopts a synthetic framework combining the adaptive signal decomposition [19] and the high-resolution time-frequency characterization, for which the empirical mode decomposition (EMD) and Hilbert transform are used respectively. The ad hoc elements contained in the EMD makes it hard to analyze mathematically. Thus, the extracted so-called intrinsic mode functions (IMFs) and subsequent TFA results tend to be physically meaningless especially when perturbated by noise. Nonetheless, this framework derives many HHT-class methods but with a solid analytical foundation, among which the synchrosqueezing transform (SST) by Daubechies et al. [20] is a well-known attempt. The SST can be regarded as a reassigned STFT/WT that sharpens approximately harmonic modes in the spectrogram/scalogram, but this scheme fails to deal with intra-wave modulated signals with the fast oscillating, not the slowly-varying amplitude and frequency. The latter is exactly the prerequisite of the SST tool [21]. Some other work has been done to obtain the modes only, without TFA for them such as the empirical wavelet transform (EWT) [22] and variational mode decomposition (VMD) [23]. They are all restricted to narrow-band modes decomposition therefore not applicable to intra-wave modulated signals having a wideband spectrum. Recently, a VMD-based method termed the variational nonlinear chirp mode decomposition (VNCMD) [24] is specifically designed for wideband multi-component signal analysis. VNCMD follows the basic idea of VMD but uses a data-driven demodulation operator to demodulate each mode before estimating its bandwidth and thus can extract modulation features with high accuracy [13]. But the initialization of VNCMD requires a given mode number and initial IF guesses for each mode, prohibiting the use of it in practical applications.

In this paper, we combine the philosophy of the HHT with that of the VNCMD to eliminate the drawbacks of two original methods. This construction leads to a descendant of VNCMD, called the iterative nonlinear chirp mode decomposition (INCMD). INCMD uses a modified VNCMD optimizer to extract the signal modes recursively (just like EMD does [11]) with the Ljung-Box Q-test result [25] as a decomposition termination criterion. According to spectral characteristics of intra-wave modulated signals [13], we obtain the peak frequency in the power spectral density (PSD) of the current signal as a constant initial IF, so that no additional IF guesses are needed. Through numerical examples, it is demonstrated that the INCMD significantly outperforms state-of-the-art techniques of the same class. Using the INCMD, intra-wave modulations can be captured with high accuracy and strong noise-robustness. These extracted modulation features by the INCMD greatly help to identify simulated nonlinear single- (S-DOF) and multi-degree-of-freedom (M-DOF) systems, as well as the real ones. Most importantly, the INCMD has a solid analytical foundation.

The structure of this paper is organized as follows. In Section 2, we briefly introduce the intra-wave modulation phenomena in nonlinear responses. In Section 3, the idea and the algorithm of the INCMD are detailed, and then a numerical example is provided to test the algorithm performance. Section 4 gives several examples including dynamic simulations and applications to real data, to demonstrate the effectiveness of our method in decomposing synthetic nonlinear responses and capturing intra-wave modulations embedded in them. Section 5 concludes this paper.

# 2. Intra-wave modulations of nonlinear responses

The modulation, including the amplitude modulation (AM) and the frequency modulation (FM), is a common phenomenon in an oscillatory signal. A well-known example is the chirp signal (see Fig. 1 (a)), which exhibits a smoothly increasing IF and a wideband spectrum as Fig. 1 (b, c) shows. Every single wave in the chirp resembles a standard harmonic, i.e., modulation occurs between waves and waves only. Herein, a single wave is called the *intra-wave*, and the relation between consecutive intra-waves is called the *inter-wave* [11]. Intuitively, the modulation in the chirp signal should be regarded as the *inter-wave modulation*, which is familiar to us.

In this sense, the definition for *intra-wave modulations* can be naturally drawn as 'the frequency/amplitude changes from time to time within a wave, its profile can no longer be a simple sine or cosine function [11]'. To demonstrate this phenomenon, an example of the Stokes wave is given in Fig. 1 (d), the profile of which is governed by the second-order perturbation solution of a nonlinear ocean system [11]:

$$x(t) = \frac{1}{2}a^{2}k + a\cos\omega t + \frac{1}{2}a^{2}k\cos 2\omega t,$$
 (1)

in which a is the amplitude and k is the wavenumber. Herein we use a=2, k=0.2, and  $\omega=2\pi\times 1/32$  rad s<sup>-1</sup>. Instead of inter-wave variations, an obvious intra-wave harmonic distortion exhibits in the Stokes wave (see blue and red lines in Fig. 1 (d)). Compared with the linear wave (i.e., the standard harmonic), the Stokes wave has a sharper crest and a flatter trough, which is related to the velocity asymmetry of deep-water waves in the real world [11]. This asymmetry leads to an intra-wave AM and FM effect. Using trigonometric identities, the perturbation solution (1) can be approximated further [12] with an intra-wave form as

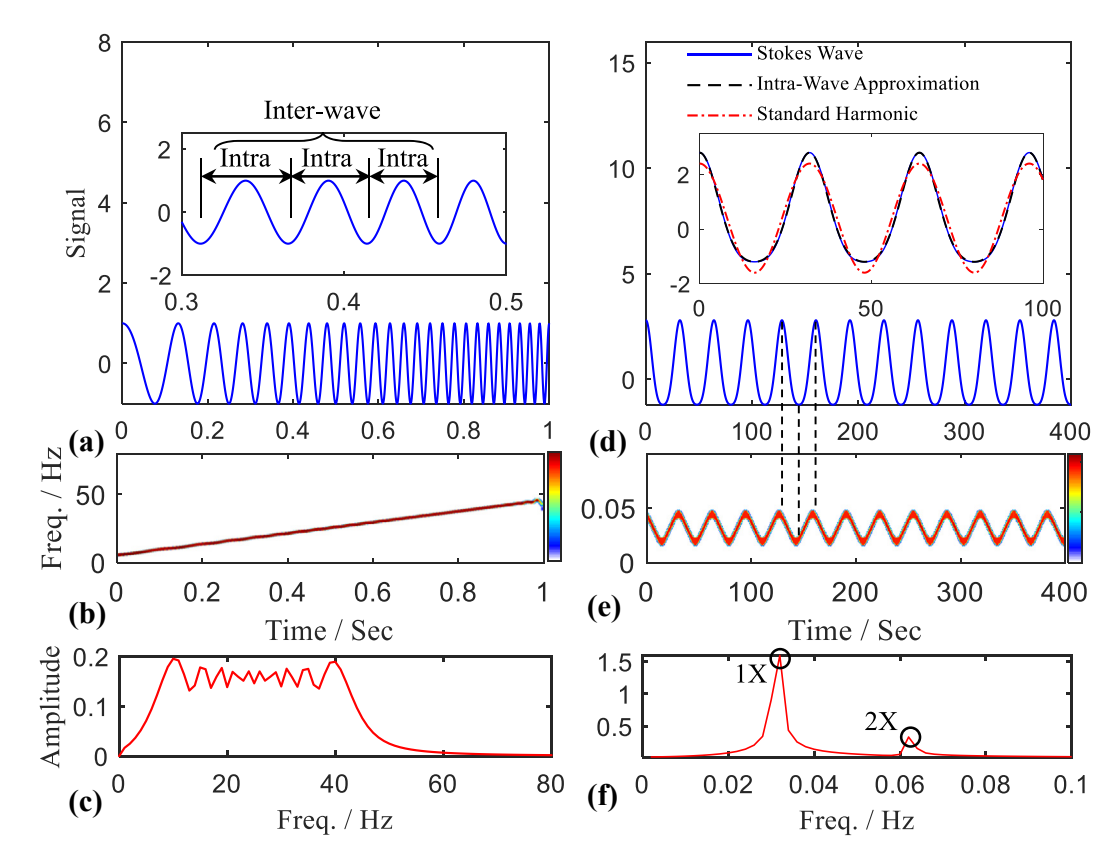


Fig. 1. The inter-wave modulated chirp and the intra-wave modulated Stokes wave [11]. (a, b, c) are the temporal waveform, HHT spectrum, and Fourier spectrum of the chirp respectively, while (d, e, f) are those of the Stokes wave.

$$\begin{split} x(t) &= a_0 + a_1 \cos \omega t + a_2 \cos 2 \, \omega t = a_0 + A(t) \cos(\omega t + \varphi(t)), \\ \text{with} \quad a_0 &= \frac{1}{2} a^2 k, a_1 = a, \ a_2 = \frac{1}{2} a^2 k \ll a_1 \ (k \ll 1), \\ \varphi(t) &= \tan^{-1} \frac{a_2 \sin \omega t}{a_1 + a_2 \cos \omega t} \approx \frac{a_2}{a_1} \sin \omega t, \\ \mathrm{IA} &\equiv a_0 + A(t) = a_0 + \sqrt{a_1^2 + a_2^2 + 2a_1 a_2 \cos \omega t} \approx a_0 + a_1 + a_2 \cos \omega t, \\ \mathrm{IF} &\equiv \frac{1}{2\pi} (\omega + \dot{\varphi}(t)) \approx \frac{1}{2\pi} \bigg( \omega + \frac{\omega a_2}{a_1} \cos \omega t \bigg), \end{split}$$

and such approximations are indeed valid (see blue and black lines in Fig. 1 (a)). The periodically oscillating IF and IA obtained in Eq. (2) is captured by the HHT spectrum as Fig. 1 (d) shows. What's worth noting is that the Fourier spectrum (see Fig. 1 (f)) only characterizes the structure of the perturbation solution, (i.e., the fundamental component (1X) and its superharmonic (2X)), which is mathematically rigorous but physically meaningless.

The mechanism of intra-wave modulations generated in the Stokes wave works in various nonlinear systems. A general mathematical model [14] for intra-wave modulated responses can be established further as

$$x(t) = a_c(1 + \varepsilon_{AM}\cos(2\pi f_{AM}t))\cos(2\pi f_c t + \varepsilon_{FM}\sin(2\pi f_{FM}t)), \tag{3}$$

the IA of which fluctuates around the center value  $a_c$  within a range of  $\varepsilon_{AM}a_c$ , while the IF fluctuates around  $f_c$  within a range of  $\varepsilon_{FM}f_{FM}$ . Two parameters  $\varepsilon_{AM}$ ,  $\varepsilon_{FM}$  control the intra-wave AM and FM degree respectively. The Bessel functions [26] can be used to expand the model signal (3) as

$$x(t) = \sum_{n=-\infty}^{+\infty} J_n(\varepsilon_{FM}) \{ a_c \cos(2\pi (f_c + nf_{FM})t) + 0.5\varepsilon_{AM}a_c \cos(2\pi (f_c + nf_{FM} + f_{AM})t) + 0.5\varepsilon_{AM}a_c \cos(2\pi (f_c + nf_{FM} - f_{AM})t) \},$$
(4)

where  $J_n(\cdot)$  is thenth-order ( $n \in \mathbb{Z}$ ) Bessel function of the first kind [26]. In the expanded signal (4), infinite harmonics exist actually. When nonlinearity gets stronger (i.e.,  $\varepsilon_{FM}$  gets larger), the response no longer has a compact support in the frequency domain since high-order Bessel functions will not attenuate then.

The Stokes wave comes from an S-DOF system. In practical M-DOF or even continuous systems, multiple modal responses are coupled, each of which leads to a wideband mode [12]. Hence, to capture such dynamics, a key issue is to decompose the raw response data into a series of physically meaningful nonlinear modes first and then extract the modulations features for each of them. Multiple intra-wave modulated modes result in an overlapped spectrum. This task is, therefore, hard to accomplish by using existing filter-bank-based decomposition techniques like the VMD [27] and EWT [22], and common TFA tools with a poor resolution like the WT and SST will also fail when dealing with fast oscillating IF and IA. Different from the HHT, VNCMD is a mathematically rigorous method for wideband multicomponent signal analysis [24], and its descendant INCMD will be introduced in the next section to make it more suitable for nonlinear data analysis.

## 3. Iterative nonlinear chirp mode decomposition (INCMD)

#### 3.1. Variational nonlinear chirp mode decomposition (VNCMD)

The VNCMD follows the basic idea of VMD [23] though, it does not require the narrow-band property of the model signal, which is the prerequisite of VMD. VNCMD is specifically designed to analyze wideband signals with multiple constituent nonlinear chirp modes (NCMs) [24], which can be expressed as

$$s(t) = \sum_{k=1}^{K} g_k(t) = \sum_{k=1}^{K} a_k(t) \cos\left(2\pi \int_{0}^{t} f_k(\tau) d\tau + \phi_k\right), \tag{5}$$

where  $a_k(t)$ ,  $f_k(t)$ ,  $\phi_k$  stands for the IA, IF and the initial phase of the k-th NCM $g_k(t)$  respectively, and K denotes the total number of NCMs. The point is that an NCM may have a wideband spectrum since its IF can vary in a wide range [24]. To estimate each NCM and extract its modulation features, a similar scheme to that used in VMD is adopted in VNCMD: demodulate each mode and minimize its bandwidth [28]. The first and also the key step in the demodulation procedure is to rewrite the signal model (5) into another form as

$$s(t) = \sum_{k=1}^{K} g_k^{d_1}(t) \cos\left(2\pi \int_0^t \tilde{f}_k(\tau) d\tau\right) + g_k^{d_2}(t) \sin\left(2\pi \int_0^t \tilde{f}_k(\tau) d\tau\right),\tag{6}$$

where  $g_k^{d_1}(t)$  and  $g_k^{d_2}(t)$  are a pair of quadrature demodulated modes of NCM $g_k(t)$  given as

$$\begin{split} g_k^{d_1}(t) &= a_k(t) \cos\left(2\pi \int\limits_0^t (f_k(\tau) - \tilde{f}_k(\tau)) d\tau + \phi_k\right), \\ g_k^{d_2}(t) &= -a_k(t) \sin\left(2\pi \int\limits_0^t (f_k(\tau) - \tilde{f}_k(\tau)) d\tau + \phi_k\right), \end{split} \tag{7}$$

from which the IA of  $g_k(t)$  can be recovered as

$$a_k(t) = \sqrt{\left(g_k^{d_1}(t)\right)^2 + \left(g_k^{d_2}(t)\right)^2}.$$
 (8)

The task here is to find the smooth function  $\tilde{f}_k(t)$ , which is exactly the estimated IF of  $g_k(t)$ , to make the obtained  $g_k^{d_1}(t)$  and  $g_k^{d_2}(t)$  in Eq. (7) have the narrowest band (i.e., the most compact spectrum [24]). The perfect  $\tilde{f}_k(t)$  is the true IF $f_k(t)$  itself, with which the FM effect in  $g_k(t)$  can be eliminated. It is worth noting that the demodulation in VMD does not involve strategies above but just acts as a frequency-shift operator (from the original band to the baseband [23]), which fails to change the bandwidth of an NCM thus cannot reveal its true modulation pattern [24].

Following the idea above, the decomposition problem in VNCMD can be formulated as a variational model [28]:

$$\begin{aligned}
& \min_{\left\{g_{k}^{d_{1}}\left(t\right)\right\}, \left\{g_{k}^{d_{2}}\left(t\right)\right\}, \left\{\tilde{f}_{k}(t)\right\}} \left\{\sum_{k=1}^{K} \left(\left\|g_{k}^{d_{1''}}\left(t\right)\right\|_{2}^{2} + \left\|g_{k}^{d_{2''}}\left(t\right)\right\|_{2}^{2}\right)\right\}, \\
& \text{sub. to } s(t) = \sum_{k=1}^{K} g_{k}^{d_{1}}\left(t\right) \cos\left(2\pi \int_{0}^{t} \tilde{f}_{k}(\tau)d\tau\right) + g_{k}^{d_{2}}(t) \sin\left(2\pi \int_{0}^{t} \tilde{f}_{k}(\tau)d\tau\right)
\end{aligned} \tag{9}$$

where the  $l_2$  norm squared of the second-order derivative is used to evaluate the bandwidth of demodulated modes [29]. The well-known alternating direction method of multipliers (ADMM) [30] is employed to address the constrained optimization problem in Eq. (9) and the detailed algorithm is given in Ref. [24].

# 3.2. An iterative version of VNCMD for nonlinear data analysis: INCMD

Two main drawbacks exist in the VNCMD method: one is that the mode number K should be given in advance, the other is that relatively good initial IF guesses for each mode are needed to start the ADMM optimizer. Priori information above is essential in a joint-optimization problem, however, hard to obtain in practical applications. To address these two issues, the INCMD, a descendant of VNCMD, is detailed next.

To eliminate the need for a known mode number K, the joint-optimization scheme is replaced herein by a step-wise approach. The INCMD uses a modified VNCMD optimizer to extract only one mode first, subtract it from the signal, and then iterate the process on the residual until a pre-set termination criterion is met [31], just like the EMD does [11]. Specifically, the variational model (9) in VNCMD is modified into

$$\min_{\substack{g_k^{d_1}(t), g_k^{d_2}(t), \tilde{f}_k(t) \\ sub. \text{ to } s_c(t) = g_k^{d_1}(t) \cos\left(2\pi \int\limits_0^t \tilde{f}_k(\tau) d\tau\right) + g_k^{d_2}(t) \sin\left(2\pi \int\limits_0^t \tilde{f}_k(\tau) d\tau\right) + g_{res},} (10)$$

where  $g_{res}$  is the residual after the k-th NCM $g_k(t)$  is subtracted from the current signal  $s_c(t)$ . The residual is, however, unknown a posterior. Adopting a greedy strategy [32,33], we obtain the desired mode by minimizing the energy of the residual in each iteration, making the NCM extracted is always the dominating mode with the highest energy in the current signal. In this vein, the modified objective function to be minimized in the discrete form can be obtained as

$$\mathscr{L}_{\rho}\left(\mathbf{g}_{k}^{\mathbf{d}_{1}}, \mathbf{g}_{k}^{\mathbf{d}_{2}}, \tilde{\mathbf{f}}_{k}\right) = \left\|\mathbf{D}\mathbf{g}_{k}^{\mathbf{d}_{1}}\right\|_{2}^{2} + \left\|\mathbf{D}\mathbf{g}_{k}^{\mathbf{d}_{2}}\right\|_{2}^{2} + \rho \left\|\mathbf{s}_{c} - \left(\mathbf{\Phi}_{k}^{1} \mathbf{g}_{k}^{\mathbf{d}_{1}} + \mathbf{\Phi}_{k}^{2} \mathbf{g}_{k}^{\mathbf{d}_{2}}\right)\right\|_{2}^{2},\tag{11}$$

where the discrete time series is  $\mathbf{t} = [t_0, t_1, \cdots, t_{N-1}]^T$ ,  $\mathbf{D}$  denotes a second-order difference matrix,  $\rho$  is a penalty coefficient, and  $\mathbf{\Phi}_k^1$ ,  $\mathbf{\Phi}_k^2$  are two phase matrices as  $\mathbf{\Phi}_k^1 = diag[\cos(\vartheta_k(t_0)), \cos(\vartheta_k(t_1)), \cdots, \cos(\vartheta_k(t_{N-1}))]$ ,  $\mathbf{\Phi}_k^2 = diag[\sin(\vartheta_k(t_0)), \sin(\vartheta_k(t_1)), \cdots, \sin(\vartheta_k(t_{N-1}))]$  in which  $\vartheta_k(t) = 2\pi \int_0^t \tilde{f}_k(\tau) d\tau$ .

The ADMM strategy is adopted to alternatively update the quadrature demodulated modes  $\mathbf{g}_k^{\mathbf{d}_1}$ ,  $\mathbf{g}_k^{\mathbf{d}_2}$  and the estimated IF  $\tilde{\mathbf{f}}_k$  in Eq. (11). First, we can easily find the optimal solutions for  $\mathbf{g}_k^{\mathbf{d}_1}$ ,  $\mathbf{g}_k^{\mathbf{d}_2}$  by letting the gradient of the objective function with respect to them be zero as

respect to them be zero as

$$\mathbf{g}_{k}^{\mathbf{d}_{1}^{*}} = \mathbf{g}_{k}^{\mathbf{d}_{1}} \Big|_{\partial \mathscr{L}_{\rho}\left(\mathbf{g}_{k}^{\mathbf{d}_{1}}, \mathbf{g}_{k}^{\mathbf{d}_{2}}, \bar{\mathbf{f}}_{k}\right) / \partial \mathbf{g}_{k}^{\mathbf{d}_{1}} = \mathbf{0}} = \left(\frac{1}{\rho} \mathbf{D}^{T} \mathbf{D} + \left(\mathbf{\Phi}_{k}^{1}\right)^{T} \mathbf{\Phi}_{k}^{1}\right)^{-1} \left(\mathbf{\Phi}_{k}^{1}\right)^{T} \mathbf{s}_{\mathbf{c}},$$

$$\mathbf{g}_{k}^{\mathbf{d}_{2}^{*}} = \mathbf{g}_{k}^{\mathbf{d}_{2}} \Big|_{\partial \mathscr{L}_{\rho}\left(\mathbf{g}_{k}^{\mathbf{d}_{1}}, \mathbf{g}_{k}^{\mathbf{d}_{2}}, \bar{\mathbf{f}}_{k}\right) / \partial \mathbf{g}_{k}^{\mathbf{d}_{2}} = \mathbf{0}} = \left(\frac{1}{\rho} \mathbf{D}^{T} \mathbf{D} + \left(\mathbf{\Phi}_{k}^{2}\right)^{T} \mathbf{\Phi}_{k}^{2}\right)^{-1} \left(\mathbf{\Phi}_{k}^{2}\right)^{T} \mathbf{s}_{\mathbf{c}}.$$
(12)

Next, the updated quadrature pair provides the increment for the IF updating (see formula (7)), which can be obtained through the arctangent demodulation technique [24] as

$$\Delta f_{k}^{*}(t) = -\frac{1}{2\pi} \frac{d}{dt} \tan^{-1} \left( \frac{g_{k}^{d_{2}}(t)}{g_{k}^{d_{1}}(t)} \right) = \frac{g_{k}^{d_{2}}(t)g_{k}^{d_{1}'}(t) - g_{k}^{d_{1}}(t)g_{k}^{d_{2}'}(t)}{2\pi \left( \left( g_{k}^{d_{1}}(t) \right)^{2} + \left( g_{k}^{d_{2}}(t) \right)^{2} \right)},$$

$$\mathbf{f}_{k}^{*} = \mathbf{f}_{k} + \left( \frac{2}{\mu} \mathbf{D}^{T} \mathbf{D} + \mathbf{I} \right)^{-1} \Delta \mathbf{f}_{k}^{*},$$
(13)

where  $\Delta \mathbf{f}_k^*$  denotes the calculated increment,  $\mathbf{f}_k^*$  is the final updated IF, and  $(2\mu^{-1}\mathbf{D}^T\mathbf{D} + \mathbf{I})^{-1}$  acts as a low-pass Wiener filter [34] to make the IF a smooth one in which  $\mathbf{D}$  is a second-order difference matrix,  $\mathbf{I}$  denotes an identity matrix, and  $\mu$  is a filter bandwidth coefficient. Finally, the k-thNCM $\mathbf{g}_k$  can be constructed using the most recently available updates as

$$\mathbf{g}_{k}^{*} = \mathbf{\Phi}_{k}^{1*} \mathbf{g}_{k}^{\mathbf{d}_{1}*} + \mathbf{\Phi}_{k}^{2*} \mathbf{g}_{k}^{\mathbf{d}_{2}*} \tag{14}$$

where  $\Phi_k^{1^*}$  and  $\Phi_k^{2^*}$  are two phase matrices formulated by  $\mathbf{f}_k^{*}$ .

The updating procedure above can be executed iteratively until no significant differences exist between the latest two results. Since decomposition of any noise makes no sense [31], the deterministic dynamics from random noise in the current signal must be distinguished before each NCM extraction. Instead of using the conventional energy-based criterion (i.e., the decomposition is stopped when the energy of the current signal is less than a pre-set threshold), we adopt the Ljung-Box Q-test [25] to assess auto-correlation in the current signal as a more physically meaningful criterion. The Ljung-Box Q-test statistic is given by [25].

$$Q(m) = N(N+2) \sum_{h=1}^{m} \frac{\widehat{\rho}_h^2}{N-h},$$
(15)

where N is the length of the observed time series, m is the maximum tested lag, and  $\hat{\rho}_h$  is the estimated auto-correlation coefficient at the lag h. Under the null hypothesis of random noise, Q(m) follows a  $\chi_m^2$  distribution [25]. The significance level is specified as 5% and we perform the test at multiple classic empirical m values at 5, 10, 15, and 20 (i.e., the null hypothesis is finally accepted only when it is accepted at all tested lags) as a relatively conservative choice [35].

As mentioned at the beginning of Sub-section 3.2, VNCMD generally employs a time-frequency distribution (TFD) ridge detection method to initialize the IF of each mode [24], which is time-consuming and not necessarily valid. Since the IF of the intra-wave modulated signal tends to fluctuate around a center value which is noticeable in the spectrum (as discussed in Section 2), we herein estimate the power spectral density (PSD) of the current signal to obtain the peak frequency as a constant initial IF to start the iteration. The Welch's method [36] is adopted here and the signal is divided into eight segments with a 50% overlap, each segment is weighted with a Hamming window.

Thus far, two issues about the unknown mode number and the IF initialization have been addressed and the whole INCMD algorithm is given in Algorithm 1. With the dynamic response data as the input, the nonlinear modes and their IFs and IAs will be the output. Nested iterative loops in the algorithm, which controls the extraction of one mode and the decomposition of the whole signal respectively, make the INCMD more stable and efficient than the original VNCMD [28].

### 3.3. Algorithm performance test

A multicomponent signal s(t) consisting of three complex modes with the inter- and intra-wave modulation in the meantime is considered to test the algorithm performance of the INCMD as

$$\begin{split} s(t) &= g_1(t) + g_2(t) + g_3(t) + n(t), \\ a(t) &= 1 + 0.3\cos(3\pi t), \quad n \sim \mathcal{N}\left(0, \sigma^2\right), \\ g_1(t) &= a(t)\cos\left(2\pi\left(-400t^4 + 800t^3 - 450t^2 + 400t\right) + 0.75\sin(40\pi t)\right), \\ g_2(t) &= a(t)\cos(2\pi(250t) + 0.75\sin(40\pi t)), \\ g_3(t) &= a(t)\cos\left(2\pi\left(-\frac{400}{3}t^3 + 200t^2 + 100t\right) + 0.75\sin(40\pi t)\right), \end{split}$$
 (16)

where  $a(t) = 1 + 0.3 \cos(3\pi t)$  governs the temporal waveform, and the IFs of three modes are IF<sub>1</sub>(t) =  $400 - 900t + 2400t^2 - 1600t^3 + 15 \cos(40\pi t)$ , IF<sub>2</sub>(t) =  $250 + 15 \cos(40\pi t)$ , and IF<sub>3</sub>(t) =  $100 + 400t - 400t^2 + 15 \cos(40\pi t)$  respectively. The signal is contaminated by Gaussian white noise n(t) with a zero mean and a standard deviation  $\sigma = 0.2$ . The simulated signal (16) is presented in Fig. 2.

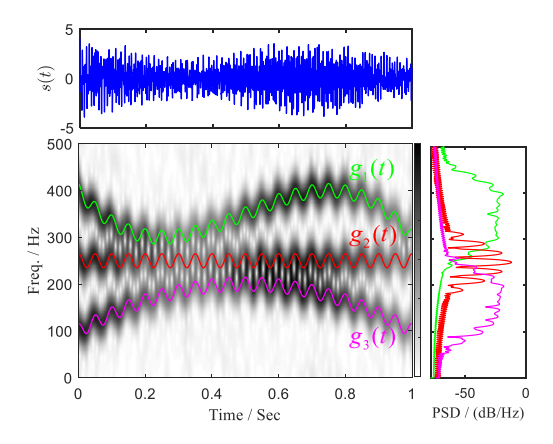


Fig. 2. A multicomponent signal consisting of three complex modes with inter- and intra-wave modulation in the meantime: figures on the top, the right, and the middle denote the synthetic waveform, the power spectrum of three modes, and the synthetic spectrogram by STFT (in which solid lines depict the true IFs) respectively.

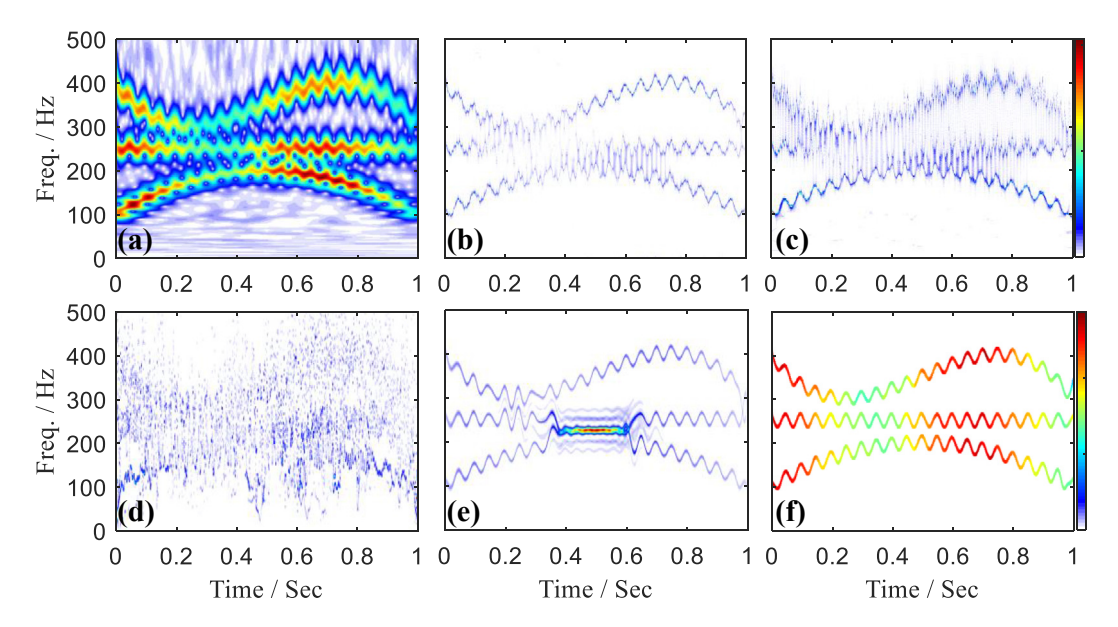


Fig. 3. The TFD of the multicomponent signal (16) by different methods. (a) Morlet scalogram. (b) F-SST spectrum. (c) W-SST spectrum. (d) HHT spectrum. (e) ICCD spectrum. (f) INCMD spectrum.

## Algorithm 1

Nested iterative loops in INCMD

```
Input dynamic response data \mathbf{s} to be analyzed Initialize parameters \rho \leftarrow 0.5, \mu \leftarrow 0.5 and the convergence threshold \varepsilon \leftarrow 10^{-8}; set the nonlinear mode counter k \leftarrow 0; let the current signal \mathbf{s_c}^0 \leftarrow \mathbf{s}; Repeat k \leftarrow k+1; Set the iteration counter i \leftarrow 0, obtain the initial IF \mathbf{f_k}^0 by Welch's PSD estimate; construct phase matrices \mathbf{\Phi}_k^{1.0} and \mathbf{\Phi}_k^{2.0} with \mathbf{f_k}^0; calculate \mathbf{g_k^{d_1,0}}, \mathbf{g_k^{d_2,0}} using (12) and \mathbf{g_k}^0 using (14); Repeat i \leftarrow i+1; Update the quadrature demodulated modes \mathbf{g_k^{d_1,i}} and \mathbf{g_k^{d_2,i}} using (12); Update the IF \mathbf{f_k}^i using (13); Construct phase matrices \mathbf{\Phi}_k^{1,i} and \mathbf{\Phi}_k^{2,i} with \mathbf{f_k}^i, update the nonlinear mode \mathbf{g_k}^i using (14), and calculate its IA\mathbf{a_k}^i using (8); Until convergence: \|\mathbf{g_k}^i - \mathbf{g_k^{i-1}}\|_2^2/\|\mathbf{g_k^{i-1}}\|_2^2 \le \varepsilon Obtain the k-th nonlinear mode \mathbf{g_k}^i, \mathbf{f_k}^i, \mathbf{f_k}^i, and update the current signal \mathbf{s_c}^k \leftarrow \mathbf{s_c}^{k-1} - \mathbf{g_k}; Until no deterministic dynamics exhibits: the null hypothesis is accepted after the Ljung-Box Q-test on the current signal \mathbf{s_c}^k Output nonlinear modes \{\mathbf{g_k}\}_{k=1,2,...} and their IFs\{\mathbf{f_k}\}_{k=1,2,...} and IAs \{\mathbf{a_k}\}_{k=1,2,...}
```

Next, different TFA methods, including WT, STFT-based SST (F-SST), WT-based SST (W-SST), HHT, a recently proposed tool called ICCD [37] and our method INCMD are employed to obtain the TFD of signal (16), as given in Fig. 3. The Morlet scalogram suffers from too poor a resolution (see Fig. 3 (a)), and the presence of the noise severely distorts the SST and the HHT spectrum as Fig. 3 (b, c, d) shows. The ICCD uses parameterized Fourier series to characterize the IF and IA of each mode [37] and shows good results in analyzing strongly modulated signals. This scheme still fails the challenge here as Fig. 3 (e) shows. The INCMD spectrum gives a satisfactory result from which three modes can be identified clearly (see Fig. 3 (f)). Fig. 4 compares the extracted modes by INCMD and those by VMD. Three nonlinear modes cannot be estimated accurately using the VMD method due to the overlapped spectrum of intra-wave modulated modes (see Fig. 2), as discussed in Section 2.

The superiority of our method in capturing intra-wave modulations becomes apparent thus far. As mentioned in Section 2, the INCMD aims to achieve a physically meaningful decomposition for nonlinear synthetic signals, making the obtained nonlinear modes and their modulation features closely related to nonlinear dynamics [38,39]. We will demonstrate this point further using all the following examples in Section 4.

#### 4. Examples

In this section, we present several examples, including dynamic simulations and applications to real data, to illustrate the effectiveness of the INCMD in decomposing nonlinear responses and capturing intra-wave modulations embedded in them. In the meantime, the superiority of nonlinearity detections and identifications based on INCMD analyses is demonstrated.

#### 4.1. Dynamic simulations

# 4.1.1. Parameter identification for S-DOF nonlinear systems

We start by considering an S-DOF Duffing oscillator in the state of damped free-vibration as

$$\begin{cases} \ddot{u}(t) + 2\zeta\omega_0\dot{u}(t) + \omega_0^2u(t) + \varepsilon\omega_0^2u^{\gamma}(t) = 0, \\ u(0) = a_0, \ \dot{u}(0) = 0, \end{cases}$$
(17)

where  $\omega_0$  denotes the linear natural frequency,  $\zeta$  is the damping ratio,  $\gamma$  stands for the order of nonlinearity,  $\varepsilon$  is a small parameter (generally  $\varepsilon$ «1) controlling the nonlinearity degree, and  $a_0$  is the initial displacement. One can obtain intra-wave modulation characteristics of such systems through a similar perturbation analysis to that used in the Stokes wave example in Section 2. A detailed discussion is provided in Ref. [12]. Appendix A gives some essential results which will be utilized in this sub-section. Since the HHT method is employed to analyze Duffing systems in many studies [12,40,41], comparisons between analysis results by the HHT and the INCMD will be a focus in this sub-section.

In the first case, the quadratic nonlinearity is generated by setting parameters as  $\zeta=0.01$ ,  $\omega_0=2\pi$  rad s<sup>-1</sup>,  $\varepsilon=0.1$ ,  $\gamma=2$  and  $a_0=1$  in Eq. (17). Fig. 5 shows the original noise-free response (blue broken lines) and its noisy version (black solid lines, contaminated by Gaussian white noise with the signal-to-noise ratio (SNR) = 20 dB; herein the SNR is computed as

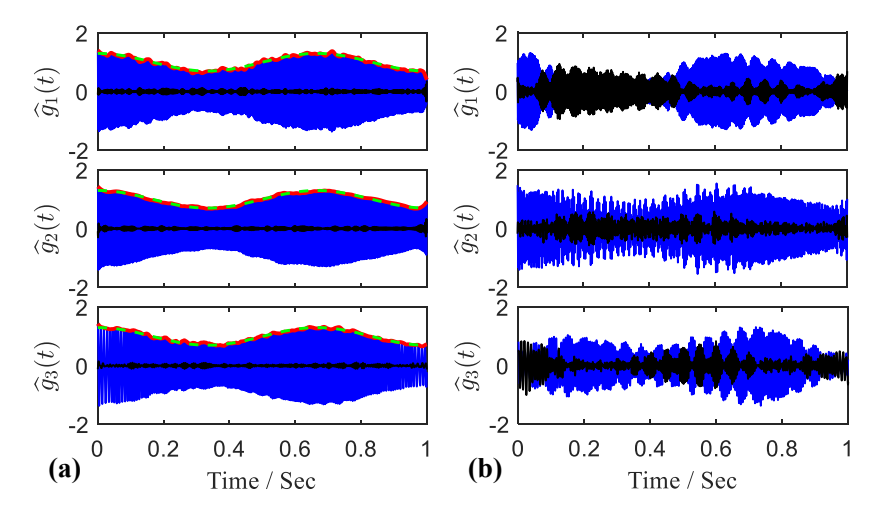


Fig. 4. Extracted modes from the multicomponent signal (16) by the (a) INCMD and (b) VMD, where the black solid lines in (a, b) are estimation errors, and the red solid lines and green dashed lines in (a) stand for the estimated IAs and true IAs respectively. (For interpretation of the references to colour in this figure legend, the reader is referred to the Web version of this article.)

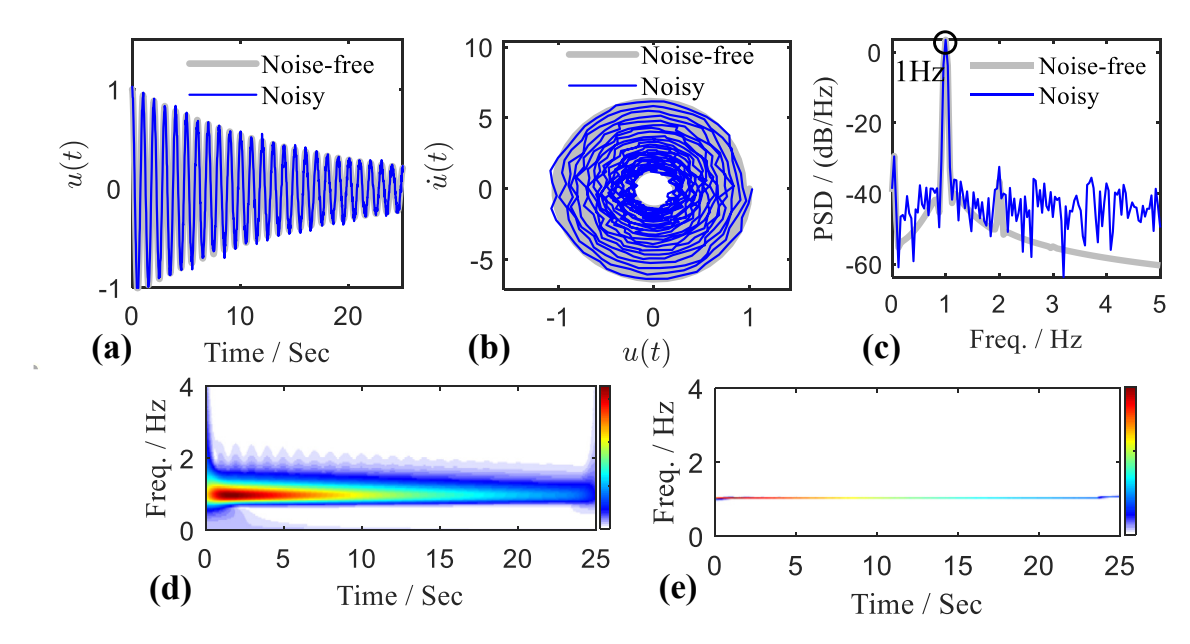
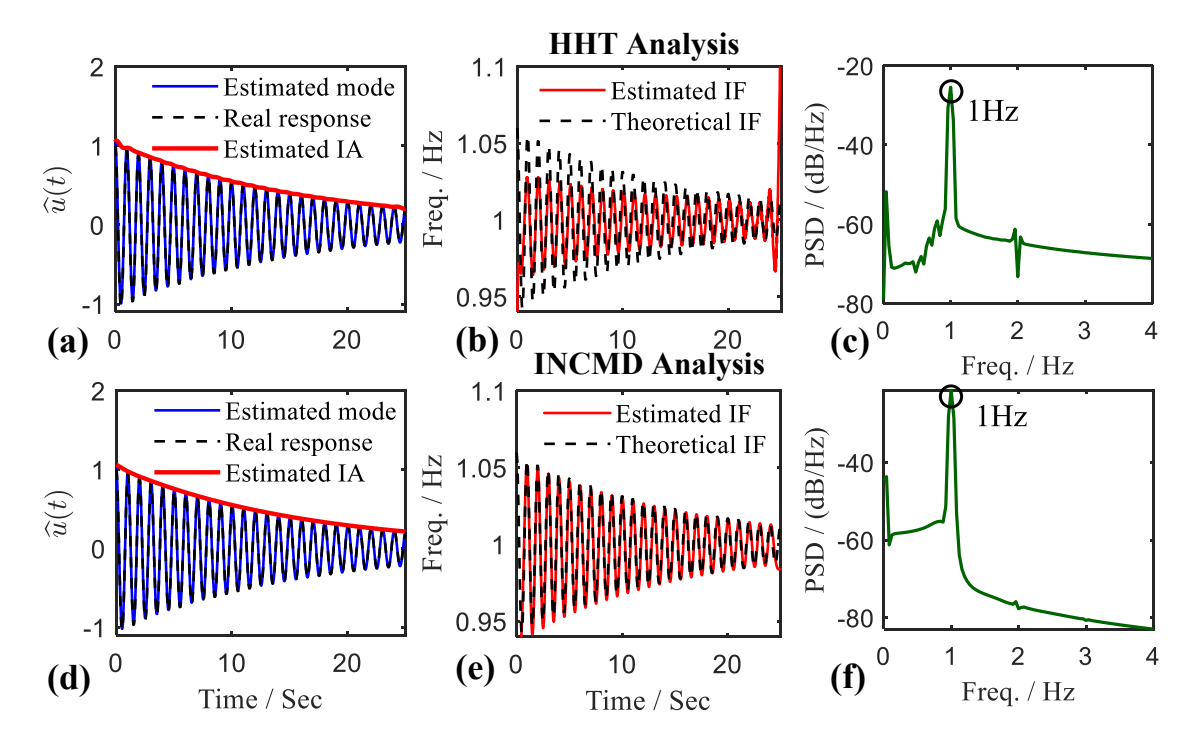


Fig. 5. A damped free-vibration response of the Duffing oscillator with quadratic nonlinearity. (a) Temporal waveform. (b) Phase diagram. (c) Power spectrum. (d) Morlet scalogram. (e) W-SST Spectrum. (a, b, c) include both the noise-free and the noisy version, while (d, e) are calculated from the noise-free response only.

 $10\log_{10}(\|u(t)\|_2^2/\|\tilde{u}(t)-u(t)\|_2^2)$ ). Traditional Fourier (see Fig. 5 (c)) or Wavelet analysis (see Fig. 5 (d, e)) can barely help in the detection of nonlinearities since these two methods can only characterize the fundamental component (i.e., linear natural frequency 1 Hz) in the response.

Comparisons between analysis results by the HHT and the INCMD are given in Fig. 6 and Fig. 7. We use the intra-wave approximation (formula (A.1)) as a theoretical reference. In the noise-free case (see Fig. 6), only one signal mode is



**Fig. 6.** Comparisons between results by the HHT and INCMD method for a damped free-vibration response of the Duffing oscillator with quadratic nonlinearity. (a, b, c) are the estimated mode, IF, and the power spectrum of the IF respectively by HHT, while (d, e, f) are those by INCMD.

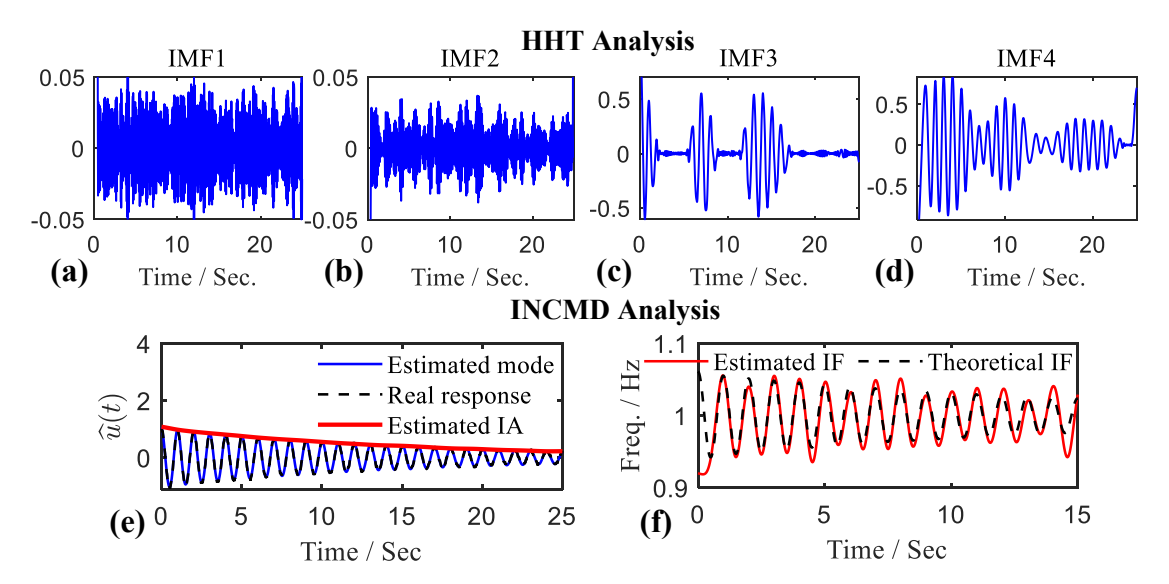


Fig. 7. Analysis results for the same response used in Fig. 6 but in a noisy environment (SNR = 20dB). (a, b, c, d) are the extracted IMFs by HHT, while (e, f) are the estimated mode and its IF by INCMD.

obtained by both two methods (see Fig. 6 (a, d)), as expected. Note that the estimated IA is a smoothly dropping one with little intra-wave modulation, which is due to the weak energy of higher harmonics in the response. The decreasing amplitude leads to a gradually weaken IF modulation (refer to formula (A.1)) as Fig. 6 (b, e) shows. A significant deviation exists between the IF estimated by HHT and the corresponding theoretical value (see Fig. 6 (b)). While using the INCMD, the real IF fluctuation pattern can be revealed with high accuracy, as shown in Fig. 6 (e).

After qualitative judgment about the existence of nonlinearity, one can determine the order and the degree of nonlinearity quantitatively by further analysis. The IF modulating frequency (which is the fundamental frequency 1 Hz in this case, see Fig. 6 (c, f)) indicates the presence of quadratic nonlinearity (refer to formula (A.1)). With this essential conclusion, one can utilize the accurately estimated IF by INCMD together with the given theoretical model in formula (A.1), to estimate the nonlinearity degree parameter  $\varepsilon$  through a least-squares fitting [12]. We also perform the same test in a noisy environment (see Fig. 7). The presence of noise leads to a severe mode aliasing in IMFs extracted by EMD, while the INCMD still works well.

Next, we consider the cubic nonlinearity (i.e., let  $\gamma = 3$  while other parameters remain unchanged, The temporal wave and spectrum of the response are not given again since no obvious differences exist between them and those shown in Fig. 5). When this is the case (see Fig. 8), the HHT suffers from end-point effects [11], while the correct modulation pattern is revealed again by INCMD. The fundamental frequency declines along with the amplitude (refer to formula (A.2)), resulting in an IF trend which should be regarded as an inter-wave mode; in the meantime, a gradually weaken IF fluctuation exhibits around this trend, denoting an intra-wave mode (see Fig. 8 (d) and refer to formula (A.2)).

Two IF modes above are coupled together. For clarity, we use the INCMD to decompose the estimated IF further, as given in Fig. 8 (e, f). The intra-wave mode can be used to determine the nonlinearity order while the inter-wave mode is the estimated skeleton curve [4] actually, with which the nonlinearity degree can be identified. Estimation results in a noisy environment are given in Fig. 9. When using the HHT, the skeleton is severely distorted and cannot even indicate the correct nonlinear type (i.e., hardening or softening, see Fig. 9 (b)). Parameter identification results in four cases above are summarized in Table 1.

Duffing oscillators are a class of essential models in engineering, nonlinear characteristics in responses tend to be submerged when nonlinearity is weak. In this example, compared with common tools (including the Fourier/wavelet analysis and the HHT), more accurate and noise-robust weak nonlinearity identification is achieved by capturing intra-wave modulations using the INCMD, especially in a noisy environment where the HHT barely works.

#### 4.1.2. Sub-systems restoration form responses of M-DOF nonlinear systems

In the second example, we investigate a 2-DOF system with a hardening and a softening Duffing oscillator coupled together [42], as Fig. 10 illustrates. The dynamic equation governing the system is

$$\begin{cases}
 m_1 \ddot{x}_1 + (c_1 + c_2) \dot{x}_1 + (k_1 + k_2) x_1 + k_4 x_1^3 - k_2 x_2 - c_2 \dot{x}_2 = 0, \\
 m_2 \ddot{x}_2 + (c_2 + c_3) \dot{x}_2 + (k_2 + k_3) x_2 + k_5 x_2^3 - k_2 x_1 - c_2 \dot{x}_1 = 0,
\end{cases}$$
(18)

with  $m_1=m_2=1$  kg,  $c_1=0.02$  N s m $^{-1}$ ,  $c_2=0.03$  N s m $^{-1}$ ,  $c_3=0.03$  N s m $^{-1}$ ,  $k_1=3\pi^2$ N m $^{-1}$ ,  $k_2=\pi^2$  N m $^{-1}$ ,  $k_3=8\pi^2$  N m $^{-1}$ ,  $k_4=9\pi^2$  N m $^{-1}$ , and  $k_5=-11.25\pi^2$  N m $^{-1}$ . The linear modal frequencies are  $f_{1n}=0.9756$  Hz and

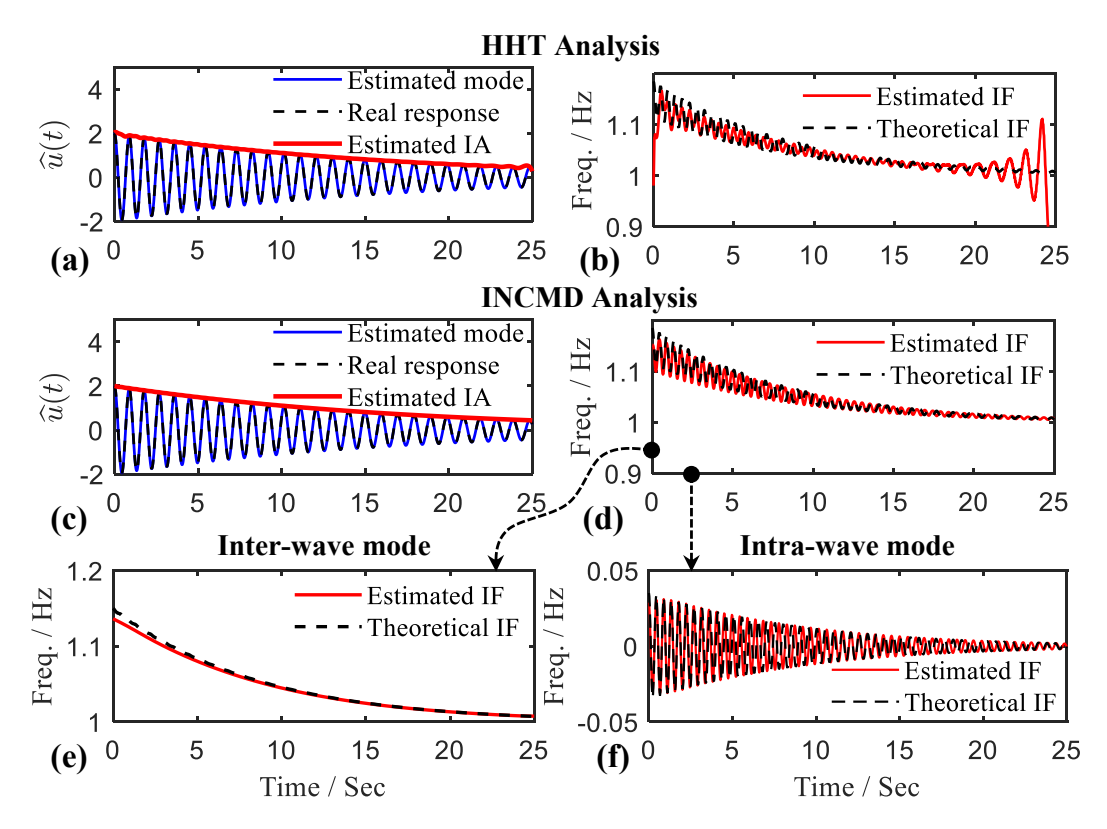


**Fig. 8.** Comparisons between results by the HHT and INCMD method for a damped free-vibration response of the Duffing oscillator with cubic nonlinearity. (a, b) are the estimated mode and its IF by HHT, while (c, d) are those by INCMD (e, f) stand for the inter- (i.e., the skeleton curve). and the intra-wave IF mode extracted further by INCMD from the estimated IF shown in (d).

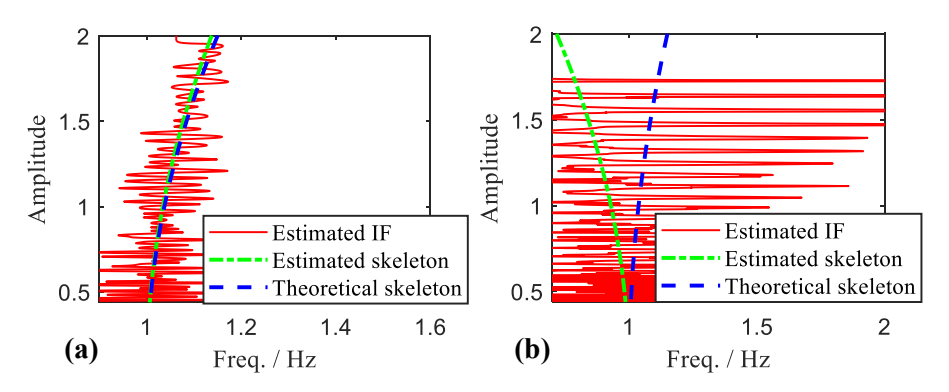


Fig. 9. Estimated skeleton curves from the same response used in Fig. 8 but in a noisy environment (SNR = 20dB). (a) By INCMD. (b) By HHT.

**Table 1** Nonlinearity degree parameter e identification results using HHT and INCMD.

Simulating case		Quadratic nonlinearity		Cubic nonlinearity	
		Noise-free	Noisy	Noise-free	Noisy
$Real_{\mathcal{E}}$		0.1		0.1	
INCMD	Identified $arepsilon$ Relative error	0.1046 4.6%	0.0898 10.2%	0.0951 4.9%	0.0916 8.4%
ННТ	Identified $arepsilon$ Relative error	0.0497 50.3%	0.0291 70.9%	0.0917 8.3%	-0.1884 288.4%

Note: In the noisy case the response is contaminated by Gaussian white noise with SNR = 20dB.

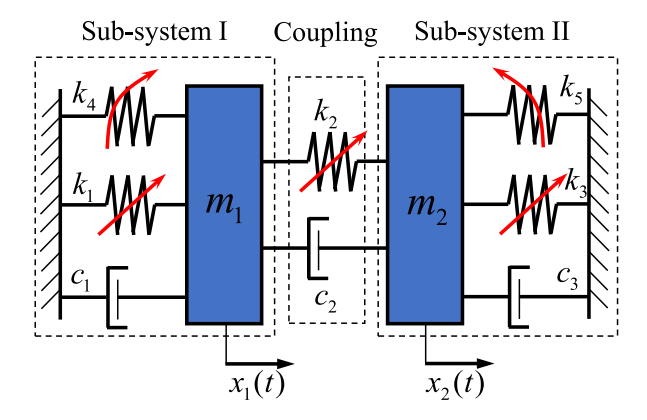
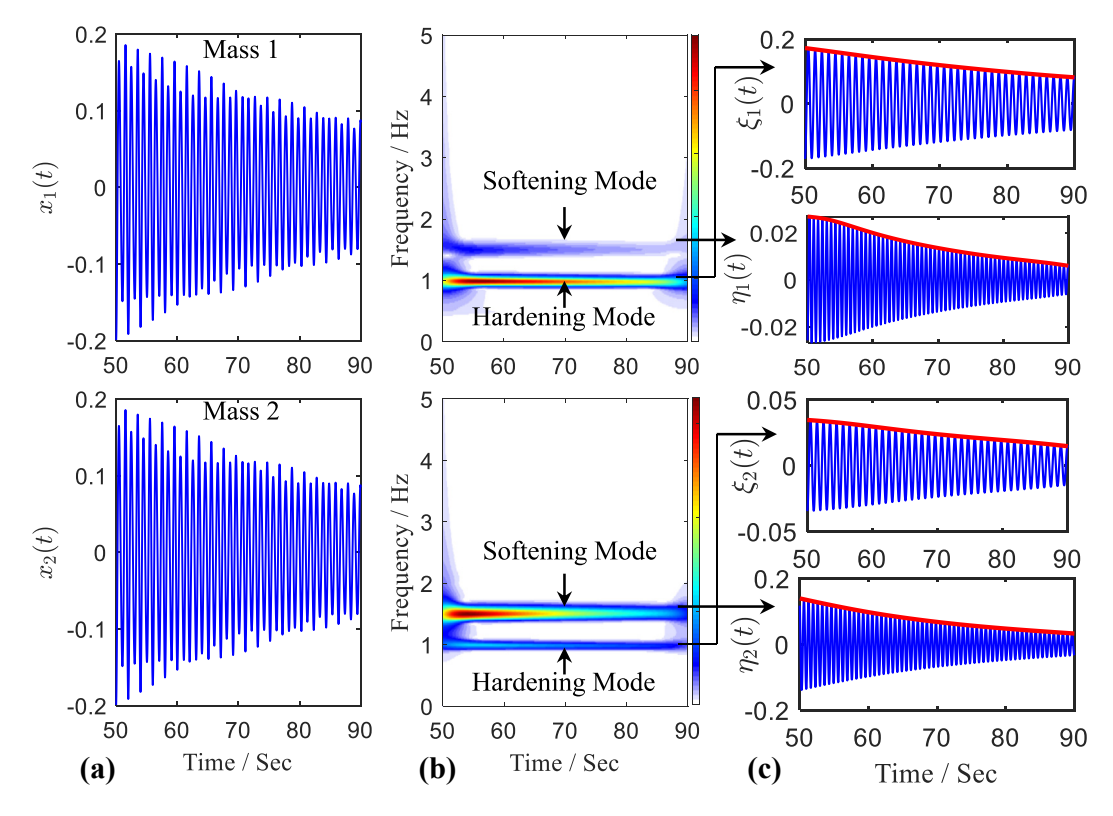


Fig. 10. The schematic view of the 2-DOF system with a hardening and a softening Duffing oscillator coupled together.

 $f_{2n}=1.5160\,$  Hz, and the linear modal shapes are  $\phi_{1n}=\{5.1930,\ 1\}^T$ ,  $\phi_{2n}=\{-0.1926,\ 1\}^T$ . The damped free-vibration response is simulated with the initial condition  $x_1(0)=1$ ,  $x_2(0)=0$ . Displacements of two masses  $x_1(t)$ ,  $x_2(t)$  are given in Fig. 11 (a).

We first employ the preliminary wavelet analysis. Natural modes centered on two linear modal frequencies can be observed in scalograms (see Fig. 11 (b)). The dominating modes which take up most of the energy in two responses differ: one is the first-order and the other is the second-order natural mode, embedding the hardening and the softening nonlinear features respectively (as will be demonstrated later). It is the coupling that gives rise to such a multiplicity of nonlinear modes in two observed motions [42].

In linear dynamics, the decoupling transformation from the physical space to the modal space creates a bridge between S-DOF and M-DOF systems [43]. Herein, the INCMD method plays a similar role. The INCMD decomposes raw responses into



**Fig. 11.** A damped free-vibration response (displacements of two masses) from a 2-DOF system with a hardening and a softening Duffing oscillator coupled together. (a) Temporal waveforms. (b) Morlet scalograms. (c) Coupled nonlinear modes (blue lines) with estimated IAs (red lines) extracted by the INCMD. (For interpretation of the references to colour in this figure legend, the reader is referred to the Web version of this article.)

four coupled nonlinear modes [44]  $\xi_1(t)$ ,  $\eta_1(t)$ ,  $\xi_2(t)$  and  $\eta_2(t)$  (see Fig. 11 (c)). Employing the skeleton extraction strategy used in S-DOF examples in Sub-section 4.1.1, one can obtain skeleton curves of four nonlinear modes together with their IFs, as given in Fig. 12 (a). The aforementioned "modal leakage" phenomenon manifests itself here: the nonlinear mode of a single sub-system spreads over the whole modal space, where a clear intra-wave FM process underlies the dominating mode (mass 1, hardening mode and mass 2, softening mode respectively). Through the modal analysis above, the modal-spatial inverse transformation is applied here to restore the initial spatial sub-systems [42]:

$$\omega_{1}^{2}(x_{1}) = \left(\phi_{\xi}\omega_{\eta}^{2} - \phi_{\eta}\omega_{\xi}^{2}\right) / (\phi_{\xi} - \phi_{\eta}), \quad \omega_{2}^{2}(x_{2}) = \left(\phi_{\xi}\omega_{\xi}^{2} - \phi_{\eta}\omega_{\eta}^{2}\right) / (\phi_{\xi} - \phi_{\eta}), 
k_{c1}(x_{1}) = \left(\omega_{\eta}^{2} - \omega_{\xi}^{2}\right) / (\phi_{\xi} - \phi_{\eta}), \quad k_{c2}(x_{2}) = \phi_{\xi}\phi_{\eta}\left(\omega_{\xi}^{2} - \omega_{\eta}^{2}\right) / (\phi_{\xi} - \phi_{\eta}),$$
(19)

where  $\omega_{\xi}$ ,  $\omega_{\eta}$ ,  $\phi_{\xi} = IA(\xi_2)/IA(\xi_1)$ ,  $\phi_{\eta} = -IA(\eta_2)/IA(\eta_1)$  are modal skeletons and the corresponding modal shapes obtained already, and  $\omega_1$ ,  $\omega_2$ ,  $k_{c1}$ ,  $k_{c2}$  are the spatial skeletons and coupling stiffness related to two initial spatial uncoupled subsystems  $m_1\ddot{x}_1 + (c_1 + c_2)\dot{x}_1 + (k_1 + k_2)x_1 + k_4x_1^3 = 0$  and  $m_2\ddot{x}_2 + (c_2 + c_3)\dot{x}_2 + (k_2 + k_3)x_2 + k_5x_2^3 = 0$ . All the variables above are functions of time.

In a rigorous sense, formula (19) is applicable only in linear dynamics. However, it also works here since nonlinearity involved in this system is relatively weak. Fig. 12 (b, c, d) shows the restored initial spatial skeletons and coupling stiffness coefficients with corresponding theoretical values. As a result, they coincide well. All the element stiffness can be further estimated using least-squares fitting and an acceptable accuracy can be achieved (see Table 2).

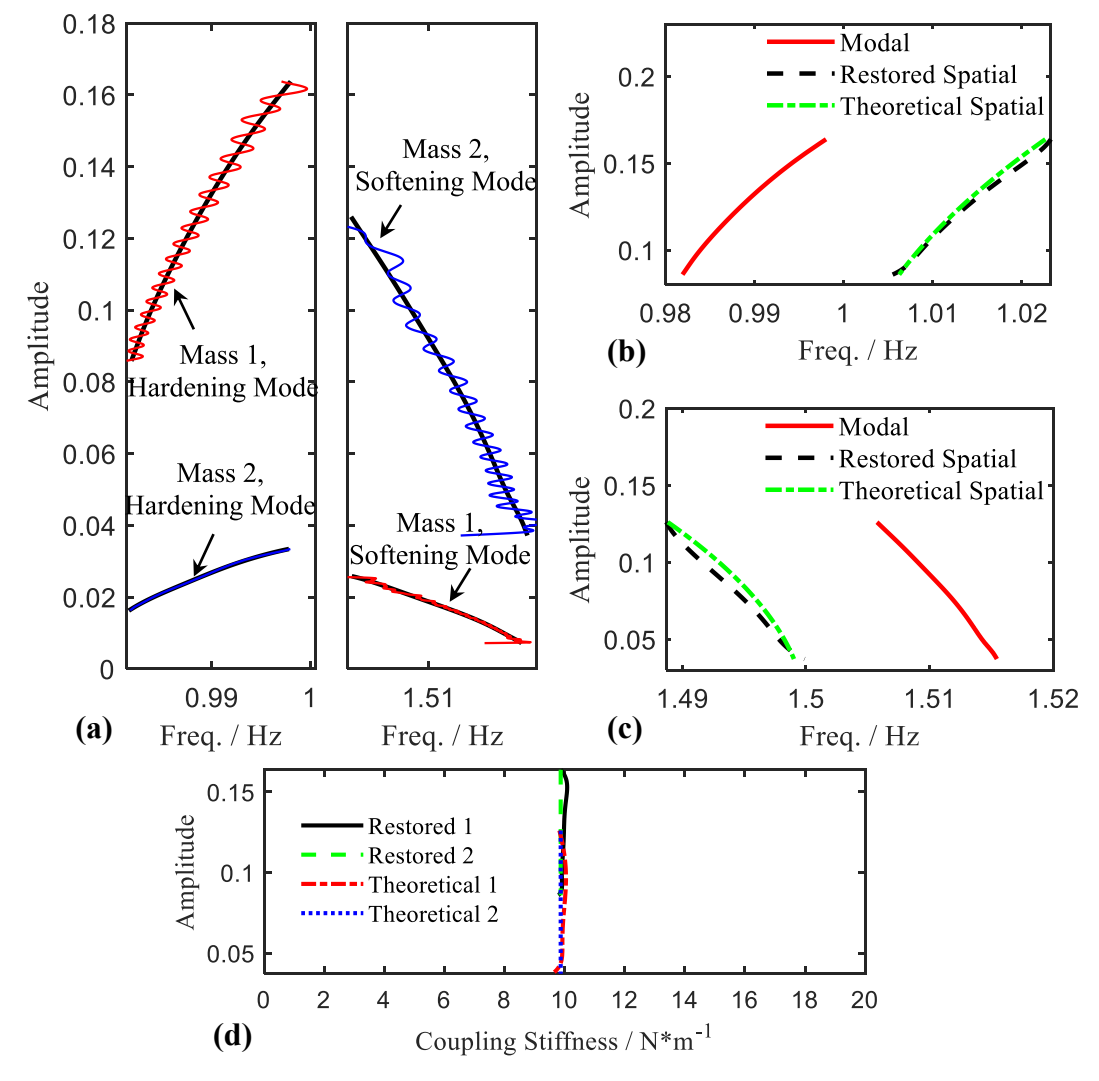


Fig. 12. Identified modal skeletons and restored initial spatial skeletons with coupling stiffness coefficients. (a) Identified modal skeletons from four decomposed nonlinear modes in Fig. 11 (c). (b, c) Restored spatial skeletons of two initial sub-systems (hardening and softening type respectively). (d) Restored coupling stiffness coefficients of two initial sub-systems.

**Table 2**Spatial sub-systems stiffness coefficients restoration results with the aid of INCMD.

	$k_1(N/m)$	k <sub>4</sub> (N/m)	k <sub>3</sub> (N/m)	k <sub>5</sub> (N/m)	k <sub>2</sub> (N/m)
Theoretical	29.6088	88.8264	78.9568	111.0330	9,8696
Restored 1	30.3185 (2.4%)	86.6057 (2.5%)	_	_	9.8846 (0.15%)
Restored 2	<b>\</b>	_	78.4612 (0.63%)	107.4799 (3.2%)	9.9136 (0.45%)

Note: Percentages in parentheses give the relative errors of the restored values.

The example in this sub-section demonstrates that when INCMD is applied to M-DOF nonlinear systems, decomposition results are physically interpretable [44]. Spatial sub-systems restoration from measured responses can be expected with the aid of the INCMD tool. HHT analysis results of two free-vibration responses are also given in Fig. 13. Either incomplete or redundant IMFs are extracted, leading to a physically unexplainable decomposition.

# 4.2. Applications to real data

## 4.2.1. Vibration response of the beam with a breathing crack

Engineering structural beams work in the state of a linear vibration generally. However, breathing cracks, a common fault caused by the beam fatigue, will result in a time-varying stiffness. In past studies, a piecewise linear (bilinear) stiffness model was extensively adopted to simulate cracked beams [45]. As Fig. 14 illustrates, the piecewise stiffness function indicating the breathing behavior of cracks, tends to fit a high-order polynomial. In this vein, the cracked beam is an S-DOF Duffing-like system. Such nonlinearity, regrettably, is very weak thus hard to capture in practice, especially in the early stages of failure. To show the effectiveness of our method in practical applications, we use the INCMD to analyze the forced-vibration response of a clamped-clamped beam with a breathing crack in this sub-section.

The experimental set-up is shown in Fig. 15. We use a 25 mm wide and 5 mm thick steel beam with a clear span of 550 mm under fixed-end boundary conditions. An electromagnetic exciter delivering a periodic impact force (set to 60 Hz) is employed. Response data are acquired using a laser displacement sensor which has a resolution of 2  $\mu$ m and a specified sampling frequency of 3000 Hz, and we use a pressure sensor to collect the real-time impact force. For comparison, we consider a healthy beam and a faulty beam with a breathing crack of 3 mm depth introduced at 350 mm from the right clamped end, respectively (see Fig. 15 (c, d)).

Fig. 16 gives forced-vibration responses of two beams. Due to the presence of the inevitable noise, two temporal waves look similar and hard to distinguish (see Fig. 16 (a, b)). In their power spectrums (see Fig. 16 (c, d)), besides the excitation frequency (1X), a rise in super-harmonics (2X and 3X) can be observed when the crack exists. Such nonlinear features are magnified by INCMD as shown in Fig. 17. Only the 1X mode has been extracted when the beam is healthy, while for the cracked beam, the response is decomposed into two intra-wave FM modes with 1X and 3X as the IF fluctuation center respectively (see Fig. 17 (a, b)). Fig. 18 gives fluctuating properties (spectrums of IFs) further, the main fluctuating frequency 1X, which is the excitation frequency, directly relates to the breathing behavior of the crack [46]. Moreover, the minor fluctuating frequency 2X (see Fig. 18 (b)) indicates a more frequent impact since crack breathing is a continuous, rather than a two-phase process demonstrated in Fig. 14 actually [45].

Nonlinear features extracted above highly agree with that of the Duffing oscillator with quadratic nonlinearity as discussed in Sub-section 4.1.1. With the collected impact force (system input) and the obtained IF and IA of the response (system output), we employ the Feldman's 'FORCEVIB' method [47] (see Appendix B for detailed procedures, which is based on the Hilbert transform originally) to verify the above conjecture.

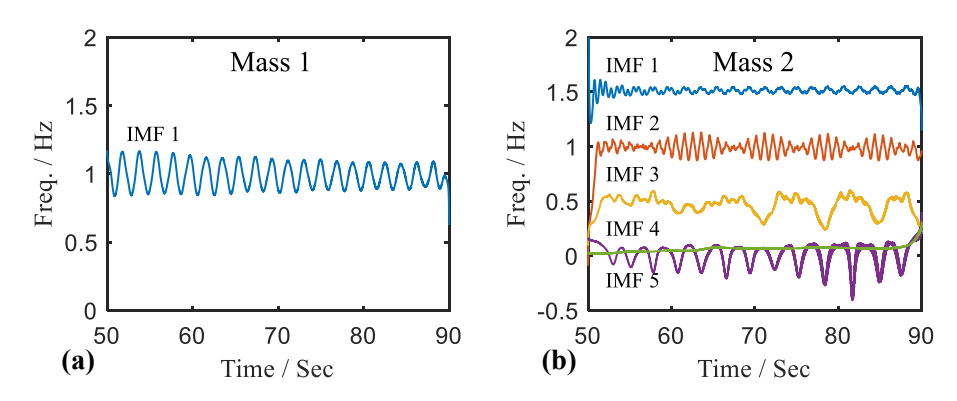


Fig. 13. HHT analysis results for two free-vibration responses in Fig. 11 (a).

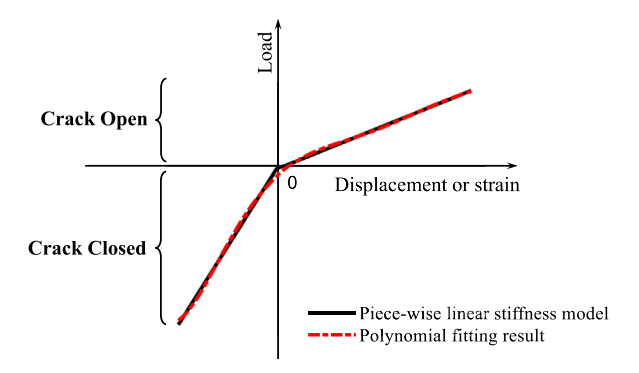
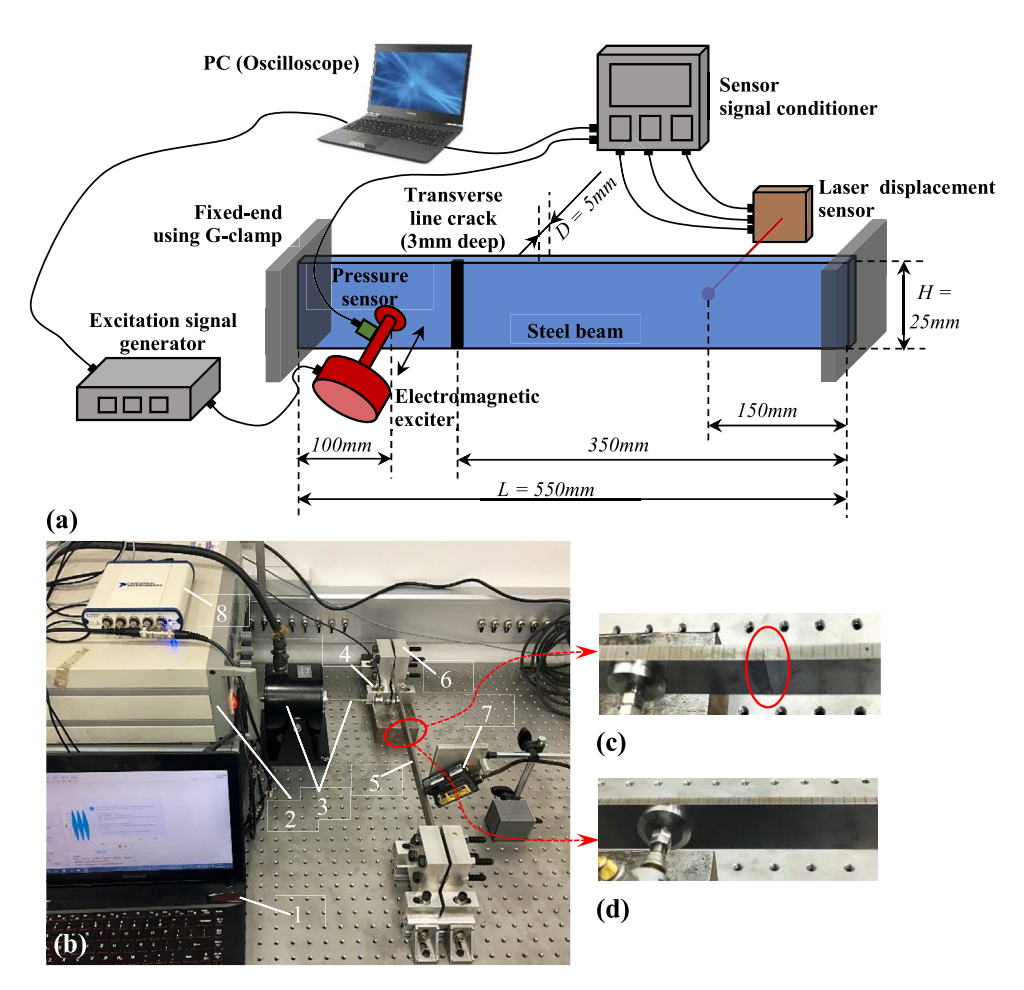
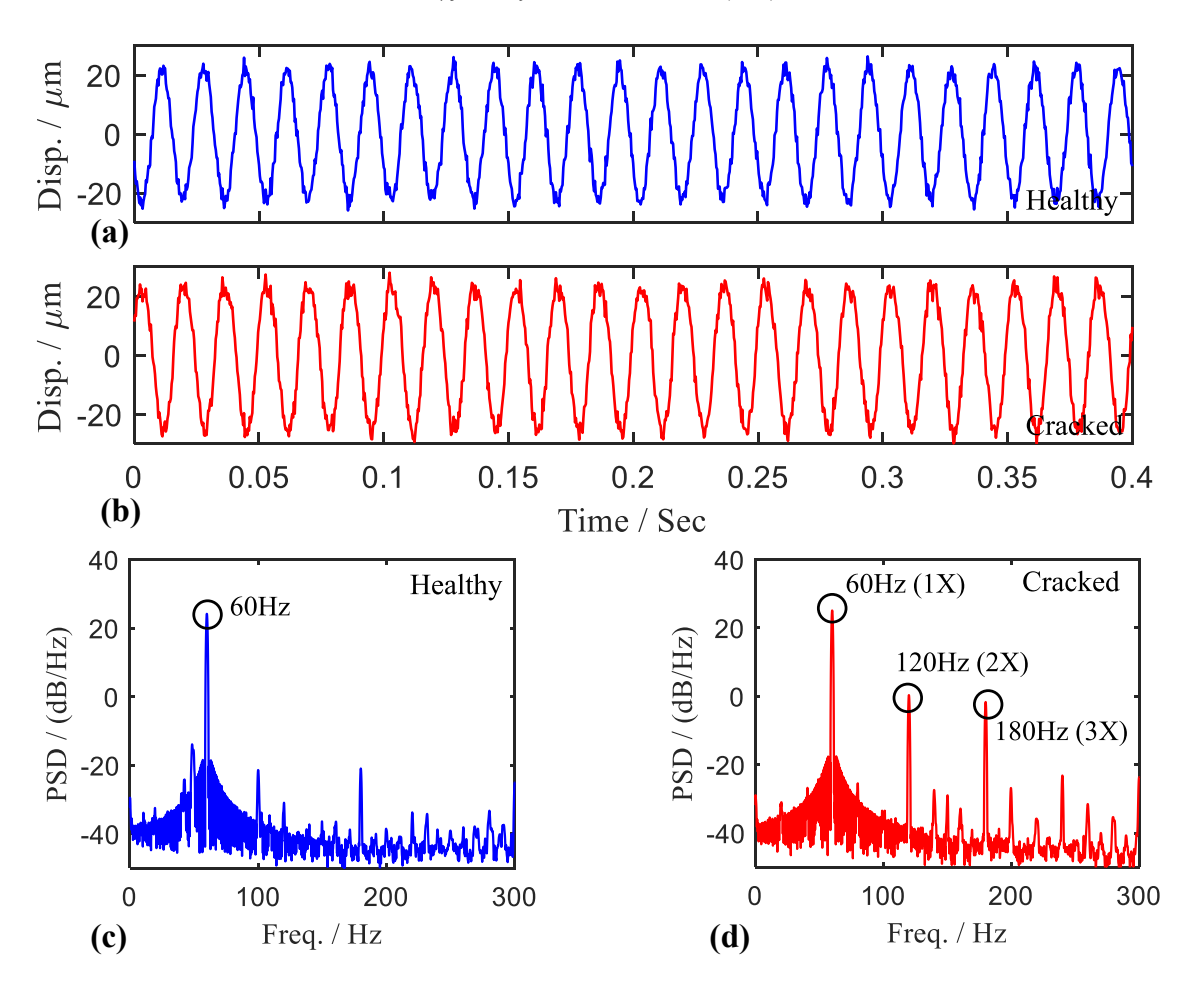


Fig. 14. The schematic load-displacement curve for a piecewise linear stiffness model [45].

The equivalent elastic and damping force of the cracked beam are obtained using the above method, as shown in Fig. 19. Next, a fitting model is to be selected to describe the nonlinear characteristic forces. An obvious hysteresis exhibits in Fig. 19 (blue lines) thus the Coulomb friction force  $\mu$ sign( $\dot{x}$ ), a typical factor inducing hysteresis loops [48], together with various types of nonlinear stiffness and damping (see Table 3) are considered as candidate models. Herein, the RMSE index (the normalized root mean square error between raw data  $\bf{f}$  and its fitting value  $\tilde{\bf{f}}$  [49]) is adopted to determine the optimal fitting model as



**Fig. 15.** Experimental setup of the beam system. (a) Schematic view. (b) Picture (1, PC; 2, excitation signal generator; 3, electromagnetic exciter; 4, pressure sensor; 5, steel beam; 6, fixed end using G-clamp; 7, laser displacement sensor; 8, sensor signal conditioner). (c) and (d) compares the healthy beam with the cracked beam by a local close-up view.



**Fig. 16.** Forced-vibration responses of two beams. (a, c) (blue lines) are the intercepted temporal waveform and the power spectrum of the response of the healthy beam, while (b, d) (red lines) are those of the cracked beam. (For interpretation of the references to colour in this figure legend, the reader is referred to the Web version of this article.)

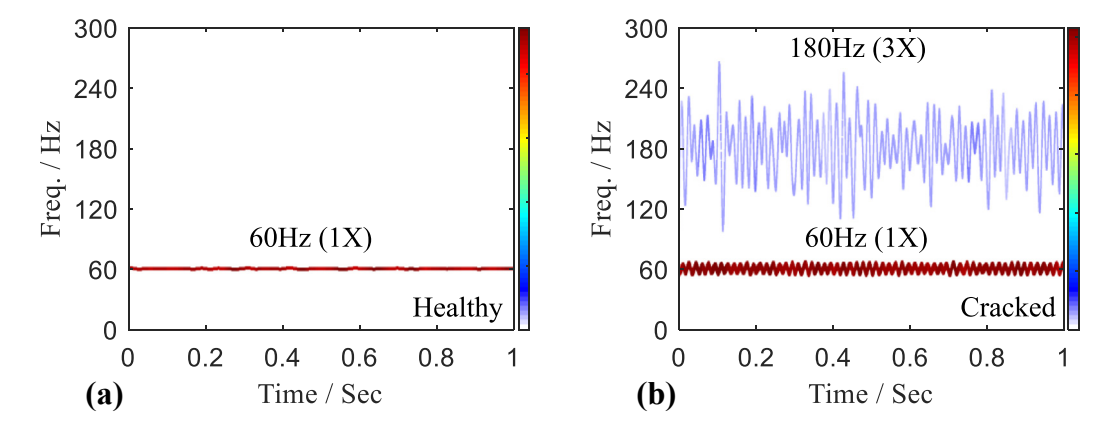
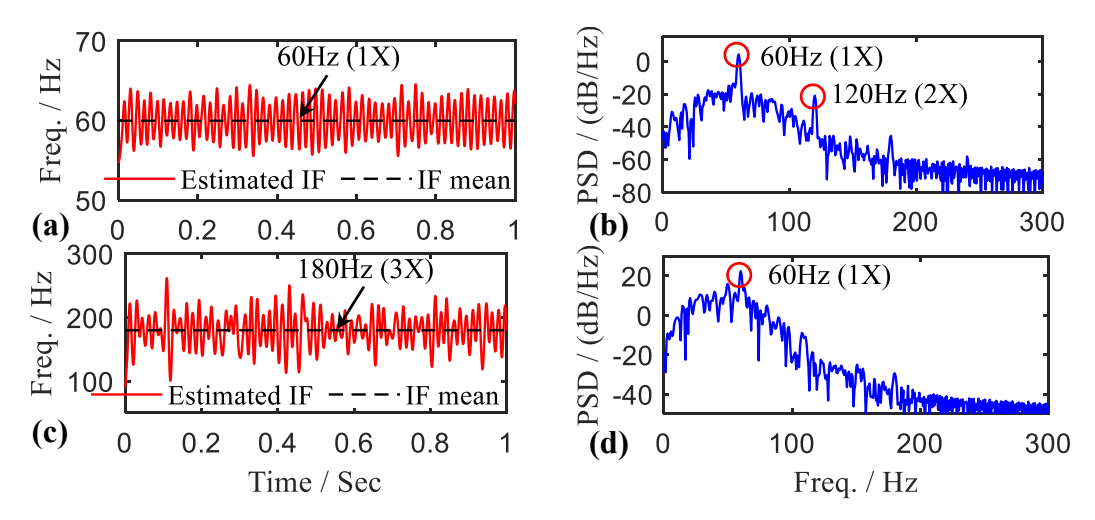


Fig. 17. TFD of the responses shown in Fig. 16 by the INCMD. (a) Healthy beam. (b) Cracked beam.



**Fig. 18.** Estimated IFs and their fluctuating properties from the cracked beam response. (a, b) are the IF and its power spectrum of 1X intra-wave FM mode, while (c, d) are those of 3X intra-wave FM mode.

$$RMSE(\tilde{\boldsymbol{f}}) = \frac{\|\boldsymbol{f} - \tilde{\boldsymbol{f}}\|_2}{\|\boldsymbol{f}\|_2},$$
(20)

where  $\|\cdot\|$  is the  $l_2$  norm of the data vector.

Table 3 gives all the fitting results, where the optimal fitting model with the minimum RMSE value is the quadratic stiffness and bilinear damping with the Coulomb friction. The finally identified mass-normalized governing equation can be represented as

$$\ddot{x} + c_{+}H(\dot{x})\dot{x} + c_{-}H(-\dot{x})\dot{x} + \mu \text{sign}(\dot{x}) + k_{1}x + k_{2}x^{2} = p(t), \tag{21}$$

where  $c_+ = 6.3915e2$ ,  $c_- = 1.3615e3$ ,  $\mu = 0.6908$ ,  $k_1 = 2.2695e6$ ,  $k_2 = 1.6893e6$ ,  $H(\bullet)$  and  $sign(\bullet)$  is the Heaviside and symbolic function respectively, and p(t) is the excitation force applied on unit mass. To check the validity of this model, responses calculated numerically using the identified model and real responses measured from the test rig are compared in Fig. 20. An excellent fit between them can be observed, which demonstrates the high accuracy of INCMD analysis results from another angle.

W-SST and HHT are also employed to analyze two responses and results are provided in Fig. 21. W-SST can only capture the fundamental component whether for the healthy or the cracked beam (see Fig. 21 (a, b)). Physically meaningless random IF oscillations are extracted by HHT from both two responses, as Fig. 21 (c, d) shows. Unsatisfactory analysis results by these two methods have necessitated the introduction of the INCMD in practical applications.

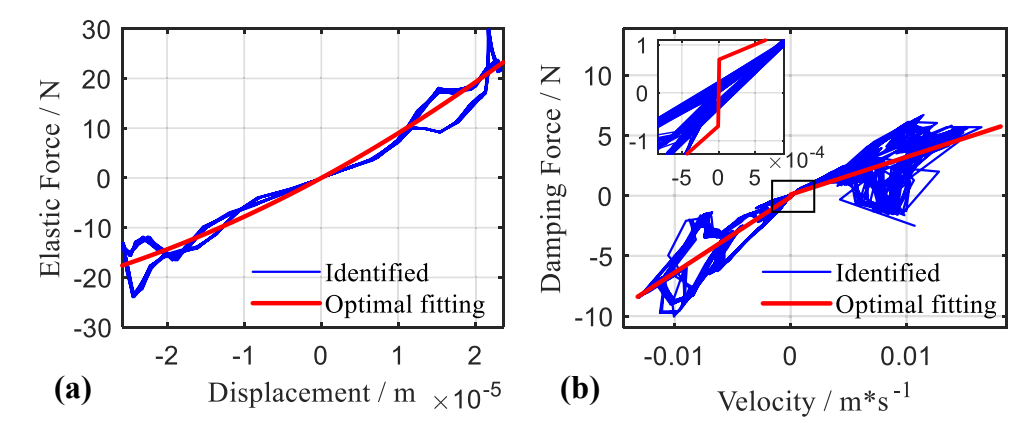


Fig. 19. Identified equivalent nonlinear characteristic forces (on unit mass). (a) The elastic force with respect to the displacement. (b) The damping force with respect to the velocity.

**Table 3**Fitting results using various nonlinear stiffness and damping models.

	Models	Estimated parameters	RMSE
Stiffness	$k_+H(x)x+kH(-x)x$	2.2695e6, 1.6893e6	0.2443
	$k_1x + k_2x^2 \star$	1.9922e6, 1.4568e10	0.1580
	$k_1 x + k_3 x^3$	1.9678e6, -2.4099e9	0.2492
	$k_1 x + k_4 x^4$	1.9679e6, 2.0604e6	0.2492
	$k_1x + k_5x^5$	1.9679e6, -5.6459	0.2492
Damping	$c_+H(\dot{x})\dot{x}+cH(-\dot{x})\dot{x}+\mu \text{sign}(\dot{x})\star$	6.3915e2, 1.3615e3, 0.6908	0.3568
	$c_1\dot{x} + c_2\dot{x} \dot{x}  + \mu \text{sign}(\dot{x})$	1.2603e3, -2.82301e4, 0.4881	0.4836
	$c_1\dot{x} + c_3\dot{x}^3 + \mu \text{sign}(\dot{x})$	1.0883e3, -1.2527e6, 0.7079	0.4838
	$c_1\dot{x} + c_4\dot{x}^3 \dot{x}  + \mu \text{sign}(\dot{x})$	9.1889e2, -2.3830e5, 1.1672	0.4855
	$c_1\dot{x}+c_5\dot{x}^5+\mu\mathrm{sign}(\dot{x})$	9.1853e2, -3.3617e3, 1.1684	0.4855

Note:  $H(\bullet)$  is the Heaviside function and sign( $\bullet$ ) is the symbolic function.  $\star$  marks the optimal fitting model with the minimum RMSE value.

#### 4.2.2. Cicada song signal

Mechanical-acoustic behavior underlies the "singing" signal of insects [50]. For instance, cicadas sing through the high-frequency vibration of their "sound box", a kind of resonant cavity structure with membranous coverings [50]. Nonlinearity may exist due to the large deformation of membranes. Herein, we apply the INCMD to a cicada song signal, which is collected outdoors through a microphone at Shanghai Jiao Tong University in June 2019 (see Fig. 22 (a)). The sampling frequency is set to 11025 Hz.

Methods like HHT and W-SST fail this challenge due to the strong noise background as Fig. 22 (b) shows, and results are not given here to save the space. Harmonic-like modes pitched at five levels are extracted by the INCMD and the residual shows no auto-correlated dynamics, as Fig. 23 (a, b, c, d) demonstrates. In this sense, the INCMD acts as an effective denoise tool. It is of interest that five modes all exhibit an oscillating IF (see Fig. 23 (d)), and the further Fourier analysis of five IFs indicates a unified modulating frequency at 30 Hz as Fig. 23 (e) shows. We cannot give an in-depth analysis of this intriguing phenomenon due to a lack of professional knowledge on entomology, but it is obvious that five modes share a common intrawave modulation mechanism, though they may come from cicadas of five different species.

#### 5. Conclusions

This paper focuses on a highly accurate, noise-robust, and mathematically solid signal processing method termed the INCMD to capture the intra-wave modulations of nonlinear responses. In the INCMD framework, the joint-optimization scheme of the VNCMD is replaced by a recursive procedure adopted in the HHT, and thus the new method becomes more adaptive without losing the rigorous mathematical foundation. Moreover, we obtain the priori IF information of the signal via the power spectrum estimation and control the decomposition termination by the result of the Ljung-Box Q-test. Both strategies are very effective and hardly increase the computational cost. Through a challenging numerical example, it has been demonstrated that our approach outperforms state-of-the-art tools of the same class such as the SST, VMD, and ICCD. Based on extracted intra-wave modulation features, the INCMD helps to accurately identify nonlinear S-DOF and M-DOF systems, including the simulated as well as the real ones. Some noteworthy conclusions are summarized as follows:

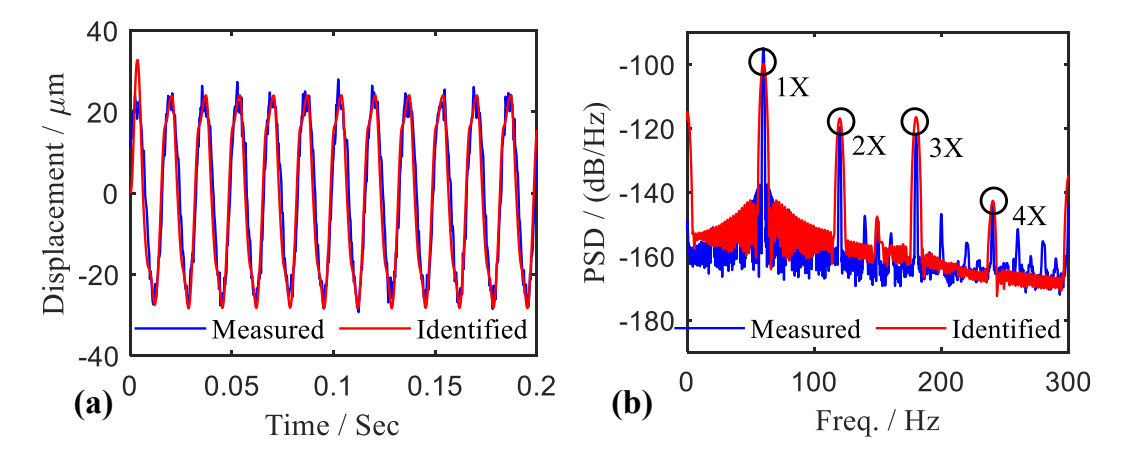


Fig. 20. The comparison between responses calculated numerically using the identified model and real responses measured directly from the test rig. (a) Temporal waveform. (b) Power spectrum.

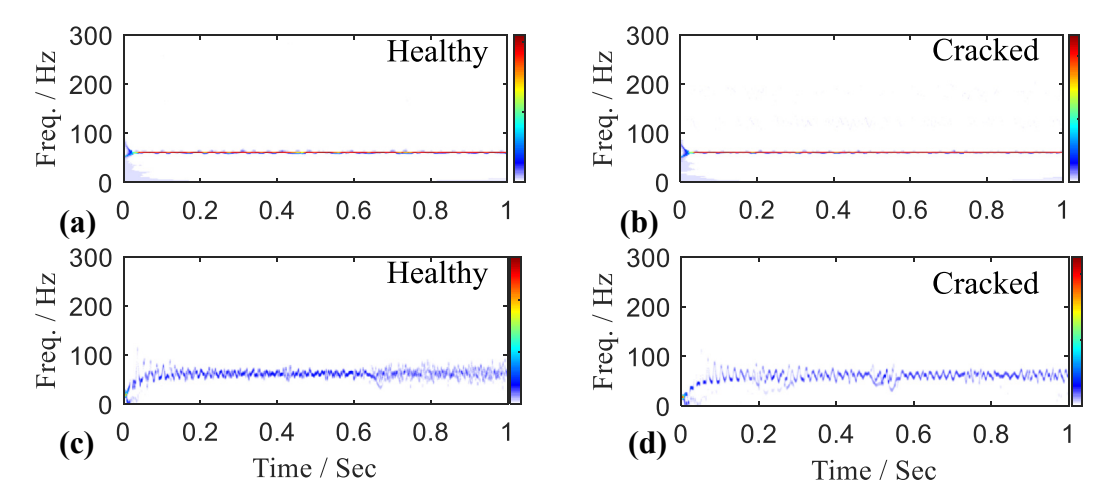


Fig. 21. TFDs of the responses shown in Fig. 16 by other methods. (a, b) are the TFD of the healthy and the cracked beam response respectively by W-SST, while (c, d) are those by HHT.

- (1) The coupled inter- and intra-wave modulations in S-DOF nonlinear systems can be separated by the INCMD, and estimation results are in good agreement with theoretical values originating from perturbation analysis, even in a noisy environment.
- (2) The INCMD decomposes responses from M-DOF systems to physically interpretable nonlinear modes [44], among which the dominating mode exhibits obvious intra-wave modulations while the minor mode (which is introduced by the coupling effect) barely does. A modal-spatial transformation [43] can be utilized to restore the initial spatial subsystems from the obtained modes.
- (3) With the aid of the INCMD, one can distinguish between the response of the healthy beam and that of the cracked beam, since the previous one is a standard harmonic process and the latter one exhibits intra-wave modulations. A valid governing equation can be identified utilizing the INCMD analysis results. The INCMD also captures the hidden intra-wave modulation pattern in a cicada song signal heavily contaminated by noise, which is very intriguing.

In all the examples, we also compare analysis results by other popular methods such as the HHT and W-SST with those by the INCMD. The W-SST tends to sharpen the fundamental modes only, ignoring inherent modulation characteristics. The HHT gives similar results to that by the INCMD but barely works in a noisy environment.

Nonlinear response data need to be carefully processed since complex dynamics underlie them. With a solid analytical foundation, the INCMD technique will be of great benefit to a rigorous verification, a thorough understanding, an accurate

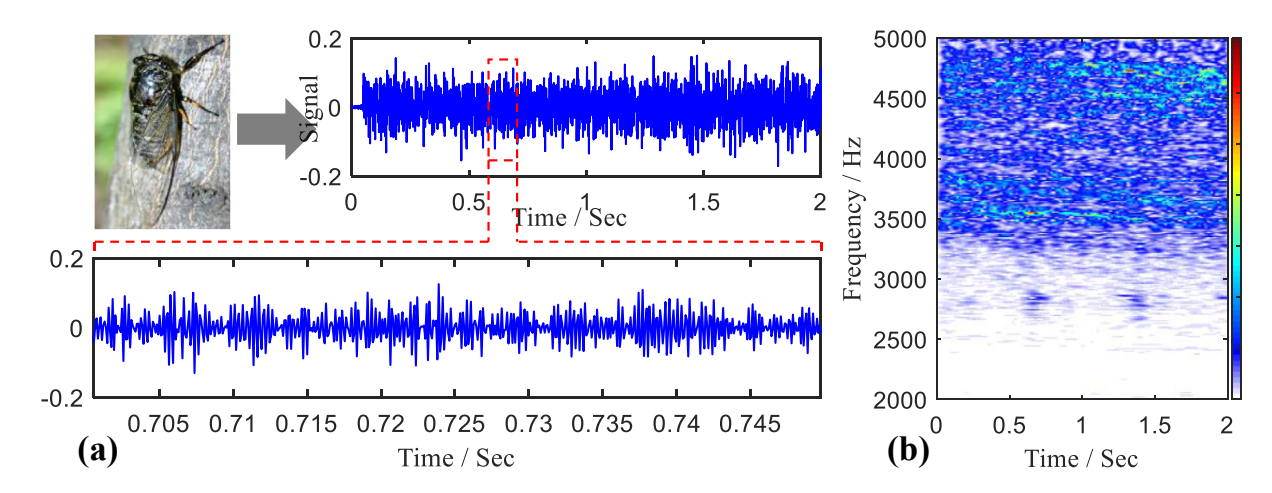


Fig. 22. The collected cicada song signal. (a). Temporal waveform. (b) Morlet scalogram.

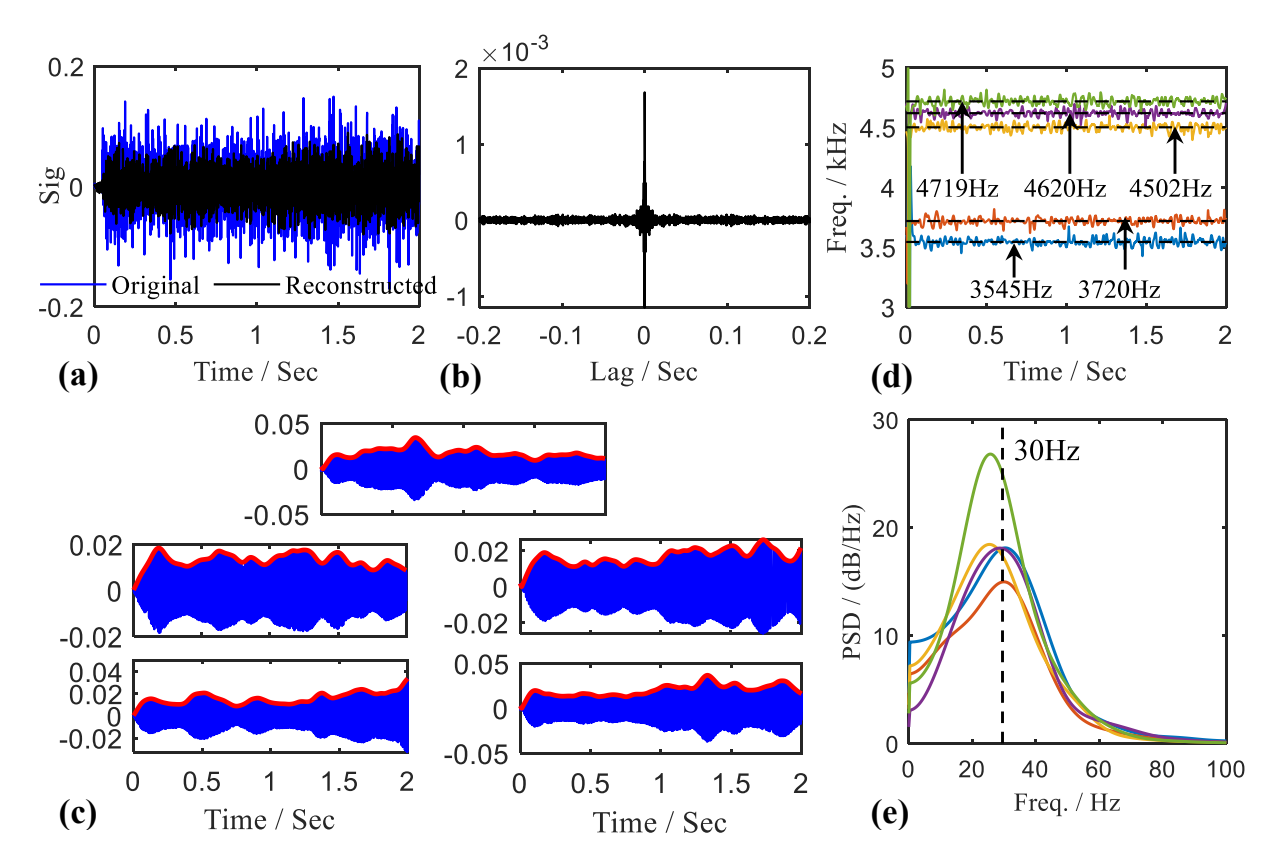


Fig. 23. The INCMD analysis results of the cicada song signal. (a) Reconstructed signal. (b) Autocorrelation of the residual. (c). Five extracted modes (red solid lines denote the IAs). (d) IFs of five modes (black broken lines stand for the mean values). (e) The power spectrum of five IFs. (For interpretation of the references to colour in this figure legend, the reader is referred to the Web version of this article.)

characterization, and a full utilization of intra-wave modulation-related nonlinear phenomena, including those already and yet to be discovered.

#### **Declaration of competing interest**

The authors declare that they have no known competing financial interests or personal relationships that could have appeared to influence the work reported in this paper.

#### **CRediT authorship contribution statement**

**Guowei Tu:** Investigation, Writing - original draft. **Xingjian Dong:** Funding acquisition. **Shiqian Chen:** Methodology, Software, Writing - review & editing. **Baoxuan Zhao:** Investigation, Data curation. **Lan Hu:** Resources. **Zhike Peng:** Supervision, Project administration.

## Acknowledgments

This work was supported by the National Natural Science Foundation of China under Grant No. 11872243 and the National Science and Technology Major Project of the Ministry of Science and Technology of China under Grant No. 2019ZX04025001. The authors thank Dr. Peng Zhou and Asst. Prof. Changming Cheng for stimulating discussions. They also thank Dr. Lei Zhang for insightful suggestions for improving the construction of this manuscript.

#### Appendix A

Intra-wave modulation features of S-DOF Duffing system responses can be obtained by perturbation analysis. Some important results utilized in Sub-section 4.1.1 in the main body are given here. For the conciseness of analyses, we omit the

damping in the system Eq. (17) (i.e., let  $\xi = 0$ ). When  $\gamma = 2$ , the intra-wave approximation of the perturbation solution is given by [12].

$$\begin{split} u(t) &= a_d + a_1 \cos \omega_1 t + a_2 \cos 2\omega_1 t = a_d + A(t) \cos(\omega_1 t + \varphi(t)), \\ \text{with } \omega_1 &= \omega_0, \ a_d = -\frac{\varepsilon a_0^2}{2}, \ a_1 = a_0 + \frac{\varepsilon a_0^2}{3} \approx a_0, \ a_2 = \frac{\varepsilon a_0^2}{6} \ll a_1, \\ \varphi(t) &= \tan^{-1} \frac{a_2 \sin \omega_1 t}{a_1 + a_2 \cos \omega_1 t} \approx \frac{a_2}{a_1} \sin \omega_1 t, \\ \text{IA} &\equiv a_d + A(t) = a_d + \sqrt{a_1^2 + a_2^2 + 2a_1 a_2 \cos \omega_1 t} \approx a_d + a_1 + a_2 \cos \omega_1 t, \\ \text{IF} &\equiv \frac{1}{2\pi} (\omega_1 + \dot{\varphi}(t)) \approx \frac{1}{2\pi} \bigg( \omega_1 + \frac{\omega_1 a_2}{a_1} \cos \omega_1 t \bigg). \end{split} \tag{A.1}$$

While for  $\gamma = 3$ , the approximation is expressed as

$$\begin{split} u(t) &= a_1 \cos \omega_1 t + a_3 \cos 3\omega_1 t = A(t) \cos(\omega_1 t + \varphi(t)), \\ \text{with} \quad a_1 &= a_0 - \frac{\varepsilon \omega_0^2 a_0^3}{32\omega_1^2} \approx a_0, \ a_3 = \frac{\varepsilon \omega_0^2 a_0^3}{32\omega_1^2} \ll a_1, \\ \underline{\omega_1} &= \sqrt{\omega_0^2 + \varepsilon \frac{3\omega_0^2 a_0^2}{4}} \approx \omega_0 \left(1 + \varepsilon \frac{3a_0^2}{8}\right), \\ \varphi(t) &= \tan^{-1} \frac{a_3 \sin 2\omega_1 t}{a_1 + a_3 \cos 2\omega_1 t} \approx \frac{a_3}{a_1} \sin 2\omega_1 t, \\ \underline{\text{Skeleton curve (Inter-wave)}} \\ &= IA \equiv A(t) = \sqrt{a_1^2 + a_3^2 + 2a_1 a_3 \cos 2\omega_1 t} \approx a_1 + a_3 \cos 2\omega_1 t, \\ \underline{\text{IF}} &\equiv \frac{1}{2\pi} (\omega + \dot{\varphi}(t)) \approx \frac{1}{2\pi} \left(\omega_1 + \frac{2\omega_1 a_3}{a_1} \cos 2\omega_1 t\right). \end{split}$$

When formula (A.1) and formula (A.2) are utilized in Sub-section 4.1.1 in the main body, the initial displacement  $a_0$  is regarded as a time-varying amplitude which approximately equals to the obtained smooth IA [12].

#### Appendix B

The Feldman's 'FORCEVIB' method [47] is introduced briefly in this section.

In the case of a forced-vibration system with weak nonlinearity, the governing differential equation can be transformed into another form as

$$\ddot{x} + h_{\dot{x}}(t)\dot{x} + \omega_{x}^{2}(t)x = p(t)/m, \tag{B.1}$$

where  $\omega_X(t)$  is the instantaneous natural frequency,  $h_{\dot{\chi}}(t)$  is the instantaneous damping, m denotes the mass of the system, and p(t) stands for the excitation force applied to the system. With the obtained envelope (i.e., IA) A(t) and the IF  $\omega(t)$  extracted from the measured displacement by signal processing method, the instantaneous damping and the instantaneous natural frequency can be estimated using the following formulas [47]:

$$\omega_{x}^{2}(t) = \omega^{2} + \frac{\alpha}{m} - \frac{\beta \dot{A}}{A\omega m} - \frac{\ddot{A}}{A} + \frac{2\dot{A}^{2}}{A^{2}} + \frac{\dot{A}\dot{\omega}}{A\omega}, \quad h(t) = \frac{\beta}{2\omega m} - \frac{\dot{A}}{A} - \frac{\dot{\omega}}{2\omega}, \tag{B.2}$$

and  $\alpha(t) = \text{Re}[P(t)/X(t)], \beta(t) = \text{Im}[P(t)/X(t)]$  are real and imaginary parts of the system output and input ratio formulated as

$$\frac{P(t)}{X(t)} = \alpha(t) + j\beta(t) = \frac{p(t)x(t) + \tilde{p}(t)\tilde{x}(t)}{x^2(t) + \tilde{x}^2(t)} + j\frac{\tilde{p}(t)x(t) + p(t)\tilde{x}(t)}{x^2(t) + \tilde{x}^2(t)},$$
(B.3)

where x(t), p(t),  $\tilde{x}(t)$ ,  $\tilde{p}(t)$  are the displacement, the excitation force, and their Hilbert transforms respectively. Then the equivalent displacement-dependent elastic force and the velocity-dependent damping force can be obtained as

$$F_{elastic}(x) = \omega_x^2(t)x(t), \quad F_{damping}(\dot{x}) = h_{\dot{x}}(t)\dot{x}(t).$$
 (B.4)

Thus, the identification of the measured nonlinear system can be achieved non-parametrically. In the original method, the IF and IA of the displacement are extracted using the Hilbert transform. Herein we use our method INCMD to estimate the IF and IA, and only the principal nonlinear mode the IF of which is centered on the fundamental frequency 1X (see Fig. 17 (b) in the main body) is considered in the identification scheme since the energy of the minor mode is weak. Prior to the system identification, the steel beam was weighed and its net mass (the beam section excited) was found to be m = 0.4219 kg.

#### References

- [1] M. Feldman, S. Braun, Nonlinear vibrating system identification via Hilbert decomposition, Mech. Syst. Signal Process. 84 (2017) 65–96, https://doi.org/10.1016/j.ymssp.2016.03.015.
- [2] S.C. Stanton, D. Culver, B.P. Mann, Tuning inertial nonlinearity for passive nonlinear vibration control, Nonlinear Dynam. 99 (2020) 495-504, https://doi.org/10.1007/s11071-019-05349-z.
- [3] H. Yao, Q. Han, L. Li, B. Wen, Detection of rubbing location in rotor system by super-harmonic responses, J. Mech. Sci. Technol. 26 (2012) 2431–2437, https://doi.org/10.1007/s12206-012-0417-4.
- [4] A.H. Nayfeh, D.T. Mook, Nonlinear Oscillations, John Wiley & Sons, 2008.
- [5] Y. Yang, Z. Peng, W. Zhang, G. Meng, Parameterised time-frequency analysis methods and their engineering applications: a review of recent advances, Mech. Syst. Signal Process. 119 (2019) 182–221, https://doi.org/10.1016/j.ymssp.2018.07.039.
- [6] Y. Yang, Z.K. Peng, X.J. Dong, W.M. Zhang, G. Meng, Nonlinear time-varying vibration system identification using parametric time—frequency transform with spline kernel, Nonlinear Dynam. 85 (2016) 1679—1694, https://doi.org/10.1007/s11071-016-2786-1.
- [7] Y. Deng, C.M. Cheng, Y. Yang, Z.K. Peng, W.X. Yang, W.M. Zhang, Parametric identification of nonlinear vibration systems via polynomial chirplet transform, J. Vib. Acoust. 138 (2016) 1–18, https://doi.org/10.1115/1.4033717.
- [8] C. Chandre, S. Wiggins, T. Uzer, Time-frequency analysis of chaotic systems, Phys. Nonlinear Phenom. 181 (2003) 171–196, https://doi.org/10.1016/ S0167-2789(03)00117-9.
- [9] Z. Feng, M. Liang, F. Chu, Recent advances in time–frequency analysis methods for machinery fault diagnosis: a review with application examples, Mech. Syst. Signal Process. 38 (2013) 165–205, https://doi.org/10.1016/j.ymssp.2013.01.017.
- [10] G. Kerschen, A.F. Vakakis, Y.S. Lee, D.M. McFarland, L.A. Bergman, Toward a fundamental understanding of the Hilbert-Huang transform in nonlinear structural dynamics, J. Vib. Contr. 14 (2008) 77–105, https://doi.org/10.1177/1077546307079381.
- [11] N.E. Huang, Z. Shen, S.R. Long, M.C. Wu, H.H. Snin, Q. Zheng, N.C. Yen, C.C. Tung, H.H. Liu, The empirical mode decomposition and the Hilbert spectrum for nonlinear and non-stationary time series analysis, Proc. R. Soc. A Math. Phys. Eng. Sci. 454 (1998) 903-995, https://doi.org/10.1098/rspa.1998.0193.
- [12] P.F. Pai, A.N. Palazotto, Detection and identification of nonlinearities by amplitude and frequency modulation analysis, Mech. Syst. Signal Process. 22 (2008) 1107–1132, https://doi.org/10.1016/j.ymssp.2007.11.006.
- [13] P. Zhou, M. Du, S. Chen, Q. He, Z. Peng, W. Zhang, Study on intra-wave frequency modulation phenomenon in detection of rub-impact fault, Mech. Syst. Signal Process. 122 (2019) 342–363, https://doi.org/10.1016/j.ymssp.2018.12.011.
- [14] A. Hu, L. Xiang, Y. Zhang, Experimental study on the intrawave frequency modulation characteristic of rotor rub and crack fault, Mech. Syst. Signal Process. 118 (2019) 209–225, https://doi.org/10.1016/j.ymssp.2018.08.051.
- [15] A.R. Messina, V. Vittal, Nonlinear, non-Stationary analysis of interarea oscillations via Hilbert spectral analysis, IEEE Trans. Power Syst. 21 (2006) 1234–1241, https://doi.org/10.1109/TPWRS.2006.876656.
- [16] A. Veltcheva, C. Guedes Soares, Nonlinearity of abnormal waves by the Hilbert-Huang transform method, Ocean. Eng. 115 (2016) 30–38, https://doi.org/10.1016/j.oceaneng.2016.01.031.
- [17] H.T. Wu, Y.H. Chan, Y.T. Lin, Y.H. Yeh, Using synchrosqueezing transform to discover breathing dynamics from ECG signals, Appl. Comput. Harmon. Anal. 36 (2014) 354–359, https://doi.org/10.1016/j.acha.2013.07.003.
- Anal. 36 (2014) 354–359, https://doi.org/10.1016/j.acha.2013.07.003.
  [18] H.T. Hsu, W.K. Lee, K.K. Shyu, T.K. Yeh, C.Y. Chang, P.L. Lee, Analyses of EEG oscillatory activities during slow and fast repetitive movements using Holo-
- Hilbert spectral analysis, IEEE Trans. Neural Syst. Rehabil. Eng. 26 (2018) 1659–1668, https://doi.org/10.1109/TNSRE.2018.2855804.
  [19] Z. Feng, X. Yu, D. Zhang, M. Liang, Generalized adaptive mode decomposition for nonstationary signal analysis of rotating machinery: principle and applications, Mech. Syst. Signal Process. 136 (2020) 106530, https://doi.org/10.1016/j.ymssp.2019.106530.
- [20] I. Daubechies, J. Lu, H.T. Wu, Synchrosqueezed wavelet transforms: an empirical mode decomposition-like tool, Appl. Comput. Harmon. Anal. 30 (2011) 243–261, https://doi.org/10.1016/j.acha.2010.08.002.
- [21] S. Wang, X. Chen, G. Li, X. Li, Z. He, Matching demodulation transform with application to feature extraction of rotor rub-impact fault, IEEE Trans. Instrum. Meas. 63 (2014) 1372—1383, https://doi.org/10.1109/TIM.2013.2283552.
- [22] J. Gilles, Empirical wavelet transform, IEEE Trans. Signal Process. 61 (2013) 3999–4010, https://doi.org/10.1109/TSP.2013.2265222.
- [23] K. Dragomiretskiy, D. Zosso, Variational mode decomposition, IEEE Trans. Signal Process. 62 (2014) 531–544, https://doi.org/10.1109/TSP.2013.
- [24] S. Chen, X. Dong, Z. Peng, W. Zhang, G. Meng, Nonlinear chirp mode decomposition: a variational method, IEEE Trans. Signal Process. 65 (2017) 6024–6037, https://doi.org/10.1109/TSP.2017.2731300.
- [25] G.M. Ljung, G.E.P. Box, On a measure of lack of fit in time series models, Biometrika 65 (1978) 297–303, https://doi.org/10.1093/biomet/65.2.297.
- [26] M. Abramowitz, I.A. Stegun, Handbook of Mathematical Functions with Formulas, Graphs, and Mathematical Tables, US Government printing office, 1948.
- [27] Y. Wang, R. Markert, Filter bank property of variational mode decomposition and its applications, Signal Process. 120 (2016) 509–521, https://doi.org/10.1016/j.sigpro.2015.09.041.
- [28] S. Chen, Y. Yang, Z. Peng, X. Dong, W. Zhang, G. Meng, Adaptive chirp mode pursuit: algorithm and applications, Mech. Syst. Signal Process. 116 (2019) 566–584, https://doi.org/10.1016/j.ymssp.2018.06.052.
- [29] S. Chen, Y. Yang, Z. Peng, S. Wang, W. Zhang, X. Chen, Detection of rub-impact fault for rotor-stator systems: a novel method based on adaptive chirp mode decomposition, J. Sound Vib. 440 (2019) 83–99, https://doi.org/10.1016/j.jsv.2018.10.010.
- [30] R.T. Rockafellar, A dual approach to solving nonlinear programming problems by unconstrained optimization, Math. Program. 5 (1973) 354–373, https://doi.org/10.1007/BF01580138.
- [31] D. Iatsenko, P.V.E. McClintock, A. Stefanovska, Nonlinear mode decomposition: a noise-robust, adaptive decomposition method, Phys. Rev. E. 92 (2015), 032916, https://doi.org/10.1103/PhysRevE.92.032916.
- [32] S.G. Mallat, Zhifeng Zhang, Matching pursuits with time-frequency dictionaries, IEEE Trans. Signal Process. 41 (1993) 3397—3415, https://doi.org/10. 1109/78.258082.
   [33] J.A. Tropp, A.C. Gilbert, Signal recovery from random measurements via orthogonal matching pursuit, IEEE Trans. Inf. Theor. 53 (2007) 4655—4666,
- https://doi.org/10.1109/TIT.2007.909108.
- [34] S.I. McNeill, Decomposing a signal into short-time narrow-banded modes, J. Sound Vib. 373 (2016) 325–339, https://doi.org/10.1016/j.jsv.2016.03.015.
- [35] G.E.P. Box, G.M. Jenkins, G.C. Reinsel, G.M. Ljung, Time Series Analysis: Forecasting and Control, John Wiley & Sons, 2015.
- [36] A. V Oppenheim, Discrete-time Signal Processing, Pearson Education India, 1999.
- [37] S. Chen, Z. Peng, Y. Yang, X. Dong, W. Zhang, Intrinsic chirp component decomposition by using Fourier series representation, Signal Process. 137 (2017) 319–327, https://doi.org/10.1016/j.sigpro.2017.01.027.

- [38] S.L. Brunton, J.L. Proctor, J.N. Kutz, Discovering governing equations from data by sparse identification of nonlinear dynamical systems, Proc. Natl. Acad. Sci. Unit. States Am. 113 (2016) 3932–3937, https://doi.org/10.1073/pnas.1517384113.
- [39] T.Y. Hou, Z. Shi, P. Tavallali, Sparse time frequency representations and dynamical systems, Commun. Math. Sci. 13 (2015) 673–694, https://doi.org/10.
- [40] P. Frank Pai, Time-frequency analysis for parametric and non-parametric identification of nonlinear dynamical systems, Mech. Syst. Signal Process. 36 (2013) 332–353, https://doi.org/10.1016/j.ymssp.2012.12.002.
- [41] M. Feldman, Hilbert transform methods for nonparametric identification of nonlinear time varying vibration systems, Mech. Syst. Signal Process. 47 (2014) 66–77, https://doi.org/10.1016/j.ymssp.2012.09.003.
- [42] M. Feldman, Identification of weakly nonlinearities in multiple coupled oscillators, J. Sound Vib. 303 (2007) 357–370, https://doi.org/10.1016/j.jsv. 2007.01.028.
- [43] D.J. Ewins, Modal Testing: Theory and Practice, Research studies press Letchworth, 1984.
- [44] S. Bellizzi, P. Guillemain, R. Kronland-Martinet, Identification of coupled non-linear modes from free vibration using time-frequency representations, J. Sound Vib. 243 (2001) 191–213, https://doi.org/10.1006/jsvi.2000.3407.
- [45] S.M. Cheng, X.J. Wu, W. Wallace, A.S.J. Swamidas, Vibrational response of a beam with a breathing crack, J. Sound Vib. 225 (1999) 201–208, https://doi.org/10.1006/jsvi.1999.2275.
- [46] B. Yang, C.S. Suh, Interpretation of crack-induced rotor non-linear response using instantaneous frequency, Mech. Syst. Signal Process. 18 (2004) 491–513, https://doi.org/10.1016/S0888-3270(03)00019-0.
- [47] M. Feldman, Non-linear system vibration analysis using Hilbert transform–II. Forced vibration analysis method 'FORCEVIB', Mech. Syst. Signal Process. 8 (1994) 309–318, https://doi.org/10.1006/mssp.1994.1023.
- [48] L. Gagnon, M. Morandini, G.L. Ghiringhelli, A review of friction damping modeling and testing, Arch. Appl. Mech. 90 (2020) 107–126, https://doi.org/10.1007/s00419-019-01600-6.
- [49] M.N. Ta, J. Lardis, Identification of weak nonlinearities on damping and stiffness by the continuous wavelet transform, J. Sound Vib. 293 (2006) 16–37, https://doi.org/10.1016/j.jsv.2005.09.021.
- [50] D.R. Hughes, A.H. Nuttall, R.A. Katz, G.C. Carter, Nonlinear acoustics in cicada mating calls enhance sound propagation, J. Acoust. Soc. Am. 125 (2009) 958–967, https://doi.org/10.1121/1.3050258.